Aus dem

Institut für Laboratoriumsmedizin

Klinikum der Ludwig-Maximilians-Universität München


# Involvement of immune cells in coagulation activated by atherosclerotic plaques

Dissertation

zum Erwerb des Doktorgrades der Medizin

an der Medizinischen Fakultät

der Ludwig-Maximilians-Universität München

vorgelegt von

Marian Radev

aus

Sofia, Bulgarien

Jahr

2025

Mit Genehmigung der Medizinischen Fakultät der
Ludwig-Maximilians-Universität München

| | |
|---|---|
| Erstes Gutachten: | Prof. Dr. Bernd Engelmann |
| Zweites Gutachten: | Prof. Dr. Jürgen Bernhagen |
| Drittes Gutachten: | Priv. Doz. Dr. Heiko Methe |
| weitere Gutachten: | |

Dekan: Prof. Dr. med. Thomas Gudermann

Tag der mündlichen Prüfung: 18.03.2025

# Contents

# Zusammenfassung

Die Atherosklerose ist eine multifaktorielle Erkrankung der arteriellen Gefäße, die aufgrund von LDL-Ablagerungen in der Intima und einer ausgeprägten Immunantwort zur Plaquebildung führt. Diese Plaques können aufgrund verschiedener Faktoren destabilisieren und reißen, was zu einem Gefäßverschluss durch eine arterielle Thrombose mit nachfolgender Ischämie führen kann.

Mittels unterschiedlicher Färbungen beobachteten wir das Vorhandensein von Cholesterinkristallen, T-Zellen, Neutrophilen und NETs in den Proben von akuten Karotiden- und Femoralisthromben sowie deren Kolokalisation mit Fibrin. In In-vitro-Experimenten zur Vollblutgerinnung wurde festgestellt, dass Cholesterinkristalle die Plaque-induzierte Thrombusbildung nicht steigern, sondern dass sie eher eine destabilisierende Funktion auf die Thrombusbildung haben können (reduzierte MAXV und Alpha-Winkel-Werte).

Homogenisiertes atherosklerotisches Plaquematerial förderte die Fibrinbildung sowohl im Vollblut als auch im thrombozytenarmen Plasma (PPP). In FXII-defizientem Plasma war die durch Plaque induzierte Fibrinbildung deutlich reduziert, was auf eine starke Beteiligung des Kontaktaktivierungssystems der Gerinnung schließen lässt.

Aktivierte klassische Monozyten förderten die Plaque-induzierte Fibrinbildung, während die nicht aktivierten klassischen Monozyten die Thrombolyse begünstigten. Nicht-klassische Monozyten zeigten keinen signifikanten Einfluss auf die Plaque-induzierte Thrombusbildung.

Nicht-aktivierte $CD4^+$ T-Zellen verzögerten die Plaque-induzierte Thrombusbildung (niedriger CFR-Wert), während aktivierte $CD4^+$ T-Zellen keinen Effekt auf die Plaque-induzierte Thrombusbildung zeigten.

Die Rolle des Fibrinolyseinhibitors PAI-1 für die plaque-induzierte Gerinnungsaktivierung wurde ebenfalls untersucht. Neutralisierung von PAI-1 induzierte eine deutliche Verlängerung der Gerinnungszeit sowie eine verzögerte Thrombusbildung, was darauf hindeutet, dass PAI-1 in den Anfangsstadien der Gerinnselbildung koagulationsfördernd wirken kann (Erhöhung der CT and MAXV-t-Werte).

## Summary

Atherosclerosis is a multifactorial disease of arterial vessels, which due to LDL deposits in the intima and pronounced immune responses inside the vessel wall can lead to plaque formation. These plaques can destabilize and rupture due to various factors, which can lead to vessel occlusion and ischemia via development of arterial thrombosis.

Using different staining techniques, we observed the presence of cholesterol crystals, T cells, neutrophils and NETs in samples from acute carotid and femoral thrombi, as well as their colocalization with fibrin. In in vitro Experiments of whole blood coagulation, we observed that cholesterol crystals do not increase the buildup of the plaque-induced thrombus but rather have a destabilizing effect on thrombus formation (reduced MAXV and alpha angle values).

Homogenized atherosclerotic plaque material promoted coagulation in whole blood as well as in platelet poor-plasma (PPP). In FXII-deficient plasma the plaque-induced fibrin formation was clearly reduced, which can lead to the conclusion that the contact activation system of coagulation is involved.

Activated classical monocytes supported plaque-induced fibrin formation, while the quiescent classical monocytes supported thrombolysis. Non-classical monocytes did not show any significant effect on plaque-induced thrombus formation.

Non-activated $CD4^+$ T cells delayed plaque-induced thrombus formation (lower CFR), while the activated $CD4^+$ T cells had no effect on the plaque-induced thrombus formation.

The role of the fibrinolysis inhibitor PAI-1 in the early stages of plaque-induced coagulation was also examined. Neutralization of PAI-1 induced a significant increase in the coagulation time and a delayed thrombus buildup, indicating that PAI-1 supported coagulation in the early stages of thrombus formation (increased CT and MAXV-t values).

# List of figures

# List of tables

# Abbreviations

**Table 1 Abbreviations**

| | |
|---|---|
| Ab | Antibody |
| alpha° | Alpha angle |
| BSA | Bovine serum albumin |
| CCs | Cholesterol crystals |
| CD | Cluster of differentiation |
| CFR | Clot formation rate |
| CFT | Clot formation time |
| cM | Classical monocytes |
| CT | Coagulation time |
| CTI | Corn trypsin inhibitor |
| CVDs | Cardiovascular diseases |
| DAPI | 4',6-diamidino-2-phenylindole |
| ddH2O | Double distilled water |
| DMSO | Dimethylsulfoxide |
| DNA | Desoxyribonucleic acid |
| DVT | Deep vein thrombosis |
| EDTA | Ethylene-diamine-tetra-acetic acid |
| FBS | Foetal bovine serum |
| FITC | Fluorescein isothiocyanate |
| FM4-64 | Fluorescent membrane 4-64 |
| GPVI | Glycoprotein VI |
| HDL-C | HDL Cholesterol |
| HEPES | 4-(2-hydroxyethyl)-1-piperazineethanesulfonic acid |
| IgG | Immunoglobulin-G |
| IHC | Immunohistochemistry |
| LDL-C | LDL cholesterol |
| LPS | Lipopolysaccharides |
| LSM | Laser scanning microscope |
| MAC-1 | Leukocyte integrin macrophage-1 antigen |
| MACS | Magnetic-activated cell sorting |
| MAXV | Maximum velocity to the widest point of the amplitude |
| MCF | Maximum clot firmness |
| ML | Maximum lysis |
| NC monocytes / nCM | Non-classical monocytes |
| NETs | Neutrophil extracellular traps |
| NK cells | Natural killer cells |
| ORN | Oligoribonucleotides |
| PAD | Peripheral arterial disease |

| | |
|---|---|
| PBMCs | Peripheral blood mononuclear cells |
| PBS | Phosphate buffered saline |
| PFA | Paraformaldehyde |
| PPP | platelet-poor plasma |
| PRP | platelet-rich plasma |
| RT | Room Temperature |
| SMCs | Smooth muscle cells |
| TEG | Thromboelastography |
| TF | Tissue factor |
| TGF-β | transforming growth factor β |
| Th | T helper |
| TL | transmission light |
| TLR | Toll-like receptor |
| TNC | Trisodium citrate |
| tPA | Tissue-type plasminogen activator |
| TPI | Thrombodynamic Potential Index |
| uPA | Urokinase-type plasminogen activator |
| uPAR | uPA receptor |
| VF | Visual field |
| vWF | von- Willebrand-factor |
| WBCs | White blood cells |
| WT | Wild type |

# I. Introduction

## 1. Atherosclerosis – Overview

Atherosclerosis is the major pathology underlying the most common cardiovascular diseases (CVDs) such as stroke, myocardial infarction, coronary and peripheral artery diseases. Atherosclerosis can be described as an accumulation of cells and fibrous material in the intima of arterial vessels that leads to the hardening and thickening of the vessel wall. The plaque (atheroma) becomes more prominent with time and can narrow the vessel lumen. If the atheroma gets destabilised or ruptures, it can lead to the formation of a thrombus (atherothrombosis).

CVDs are the leading cause of death in the world, with an estimated 17.9 million people worldwide having died from CVDs in 2019. This number represents 32% of all global deaths. Of these deaths, 85% were caused by stroke or heart attack (Table 2)[1, 2].

| Global CVD-related deaths in 2019 | |
|---|---|
| Cause | Percentage (%) |
| Cardiovascular diseases (total) | 32.84% |
| Ischaemic heart disease | 16.17% |
| Stroke | 11.59% |
| Hypertensive heart disease | 2.05% |
| Cardiomyopathy and myocarditis | 0.60% |
| Atrial fibrillation and flutter | 0.56% |
| Peripheral artery disease | 0.13% |
| Other cardiovascular and circulatory diseases | 0.49% |

**Table 2 Global death contribution of CVDs – 2019**
Percentages of deaths contributed by CVDs worldwide in 2019. Please note that not all deaths are necessarily linked to atherosclerosis but may be, for example, a consequence of hypertension. Source: Global Burden of Disease (GBD) - https://www.healthdata.org/gbd/2019

There are multiple risk factors which can promote atherosclerosis including tobacco use, high alcohol intake, an unhealthy diet, lack of physical activity, arterial hypertension, as well as hyperlipidaemia[3]. Atherosclerotic CVDs can cause ischaemic complications such as myocardial infarction or less severe conditions such as angina pectoris. Atherosclerosis can also cause ischaemic stroke or transient ischaemic attacks by hindering the blood supply to the brain. It can also lead to malformations in the arterial vessel system, compromising vessel wall structure and contributing to the formation of aneurysms. When the peripheral arteries are affected, intermittent claudication can also occur (peripheral arterial disease), which ultimately leads to critical ischaemia[4].

## 2. Initiation of atherosclerosis

The onset of atherosclerosis is subclinical without any evident symptoms. A major contributing factor to the formation of atherosclerosis is LDL cholesterol (LDL-C). The exposure of the vessel wall to pathologically high cholesterol levels[5,6] is the single most important factor for the onset and progression of atherosclerosis[7]. The fact that patients with familial hypercholesterolemia develop atherosclerotic CVDs early in their lives supports the causal role of LDL-C[8].

On the other hand, HDL cholesterol (HDL-C) is traditionally thought to be associated with a lower risk of developing CVDs, although genetic evidence does not entirely support this assumption and multiple therapies involving increasing the levels of HDL-C have failed to reduce the risk of atherosclerosis[9,10]. The involvement of other atherosclerotic risk factors such as smoking or hypertension in the progression of CVDs is not yet fully understood. Atherogenic factors are in general associated with chronic inflammation of the intima which can promote atherosclerosis[11].

### 2.1 Endothelial changes and atheroma formation

A major trigger of the initiation of atherosclerosis is local damage to the endothelium and the disruption of its function[12-14]. The atherosclerotic plaque then tends to form mostly at sites with non-laminar blood flow properties[15]. Changes to the endothelial phenotype can also lead to enhanced expression of adhesion molecules and chemokines which attract leukocytes and promote their entry into the intima[12-14]. Moreover, due to the accumulation of cells and plaque material, the anti-thrombotic properties of the endothelium are impaired (Figure 1)[16,17].

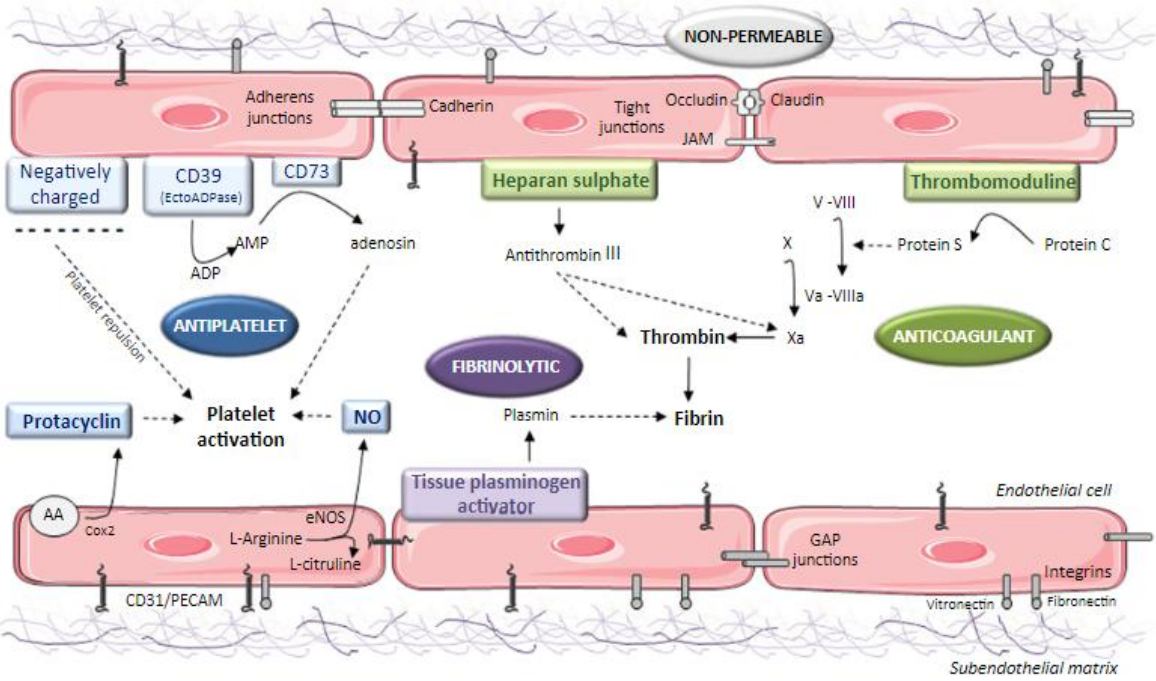


**Figure 1 Anti-thrombotic properties of healthy endothelium**
Under normal physiological conditions, the endothelium expresses multiple molecules with antiplatelet (blue), anticoagulant (green) and fibrinolytic (purple) properties.
Source: Badimon et al. 2014


The formation of the atheroma begins with the deposition of LDL particles in the intima. Once inside the intima, these particles undergo additional modifications transforming into oxidised LDL-C making them more proinflammatory and immunogenic. Multiple immune cells such as monocytes, mast cells, neutrophils, natural killer cells and dendritic cells are recruited to the intima, at the site of LDL particle deposition[16]. There is some evidence that non-classical monocytes can antagonise the inflammatory nature of classical monocytes and help recruit neutrophils through the secretion of TNF-α and thus promote vessel restitution[18]. Additionally, T helper (Th)1 and Th2 cells, as well as autoantibodies (for example against peptides of apolipoprotein B-100) are also critical to the progression of atherosclerosis. Moreover, cytokines such as IL-18 further promote progression of the atherosclerotic lesion[19-21].

The monocytes recruited to the intima differentiate and begin to phagocytize the LDL-C particles, ultimately becoming foam cells as they are unable to cope with the load of LDL-C and undergo apoptosis[22]. This process can further intensify the inflammation and progression of the atherosclerotic lesion. Nonetheless some resident macrophages and foam cell subsets can have anti-inflammatory functions and can assume an atheroprotective role hindering the atheroma development[23,24]. Additionally, smooth muscle cells (SMCs) migrate from the media into the intima in part due to cytokines released by the activated leukocytes (Figure 2)[25].

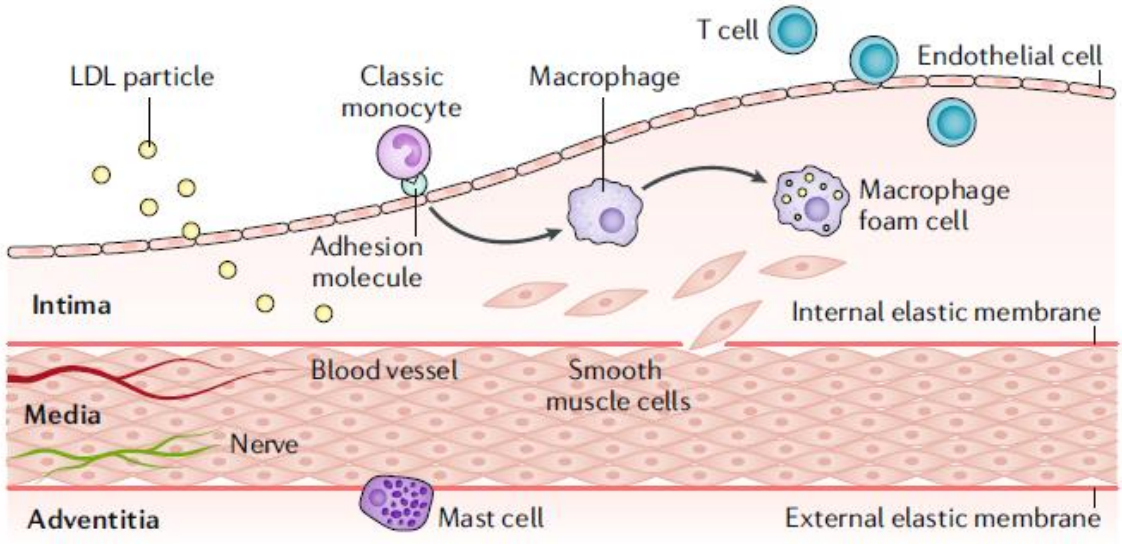


**Figure 2 Atherogenesis**
Schematic representation of atherogenesis: LDL particle and monocyte invasion into the intima. Subsequent macrophage differentiation and LDL uptake. SMCs migration from the media to the intima due to mediators released from the activated leukocytes.
Source: Libby P. et al. 2019, *Copyright © 2019 Springer Nature Limited*
Reproduced with permission from Springer Nature

## 2.2 Progression of atherosclerosis and immune cell involvement

Once an atheroma has formed, it continues to grow by accumulating more lipids and lipid-engulfing cells. These cells can be monocytes from the bloodstream which upon migration into the vessel wall differentiate into macrophages or smooth muscle cells, which when stimulated by the chemokines migrate and proliferate taking on a macrophage-like phenotype. Several types of T cells are also known to be present within the atheroma. T cells can both promote and inhibit the development of the atherosclerotic plaque. For example, Th1 cells can promote plaque progression through IFN-γ, whereas Th2 (through IL-4/5/13) can act to dampen inflammation when exposed to cytokines such

as IL-10. Th9, $T_{fh}$ cells as well as the CD28-negative subclass of T cells ($CD28_{null}$) act pro-inflammatory and contribute to the progression of the plaque (Figure 3). Another subset of T cells that can limit plaque growth and reduce inflammation are the $T_{reg}$ cells, through their ability to secrete transforming growth factor β (TGF-β)[26,27]. Also, the TR1 T cell subclass has been shown to stabilise the plaque and dampen inflammation mostly through mediation of IL-10. Th17 cells have been observed to have mixed effects on atheroprogression as they can act both pro-atherogenic and atheroprotective. Parts of the atheroma that reach the local lymph nodes can also act as antibodies against LDL particle components, promoting B cells differentiation into plasma cells and further driving inflammation[28].

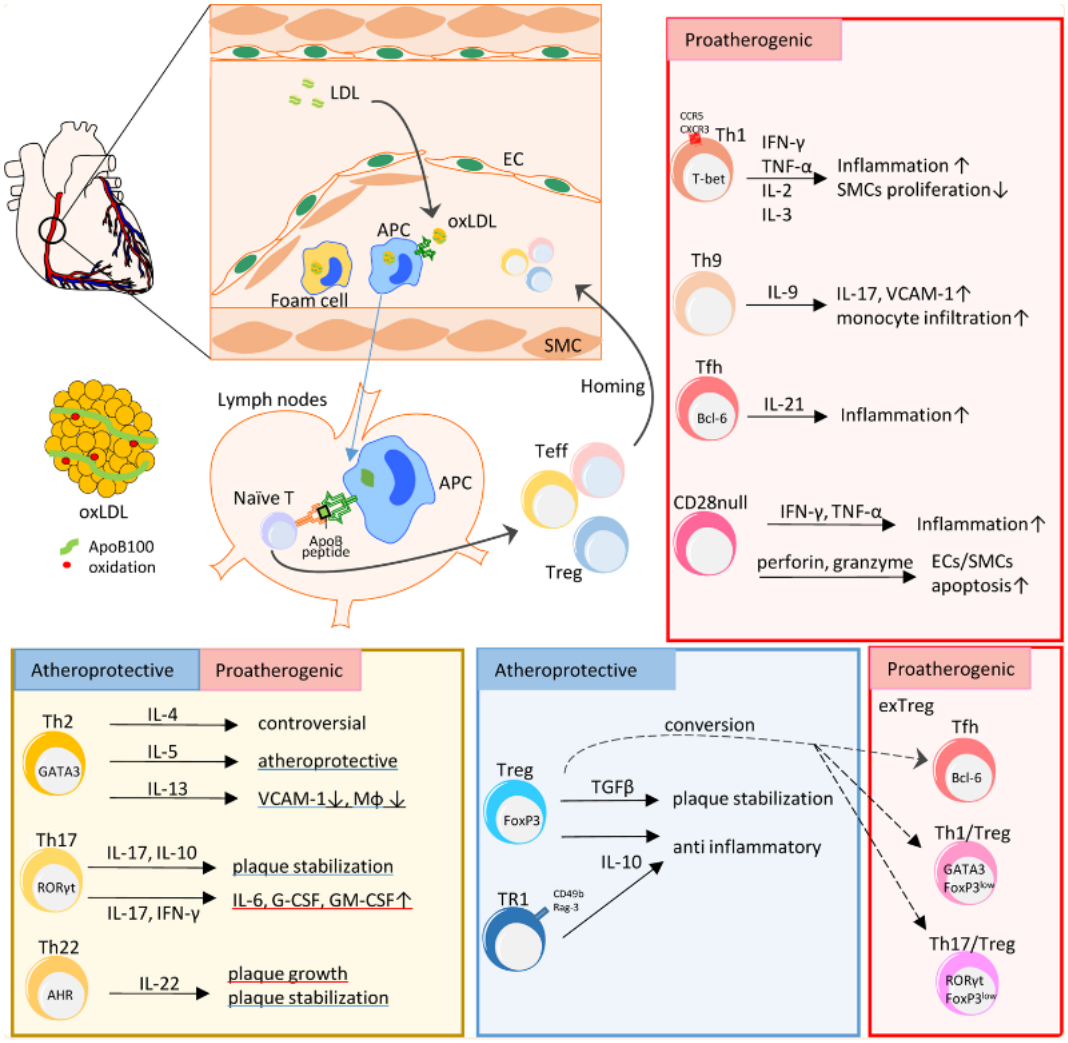


**Figure 3 Role of T cells in atheroma development**

Depicted are the diverse types of T helper cells present in atherosclerotic plaques and their effects on atherogenesis.

Another major contributor to plaque growth is the extracellular matrix substance released by the SMCs (Figure 4)[29]. Macrophage-like SMCs that have taken up lipid particles can undergo apoptosis, and thereby contribute to the formation of a lipid-rich and later a necrotic core, mostly through insufficient efferocytosis[30], further advancing the atheroma (Figure 4)[31]. Not only do these cells contribute to atheroma buildup but also in the later stages of atherothrombosis, by expressing high levels of tissue factor (TF), are a major promoter of plaque-induced thrombosis[32-34].

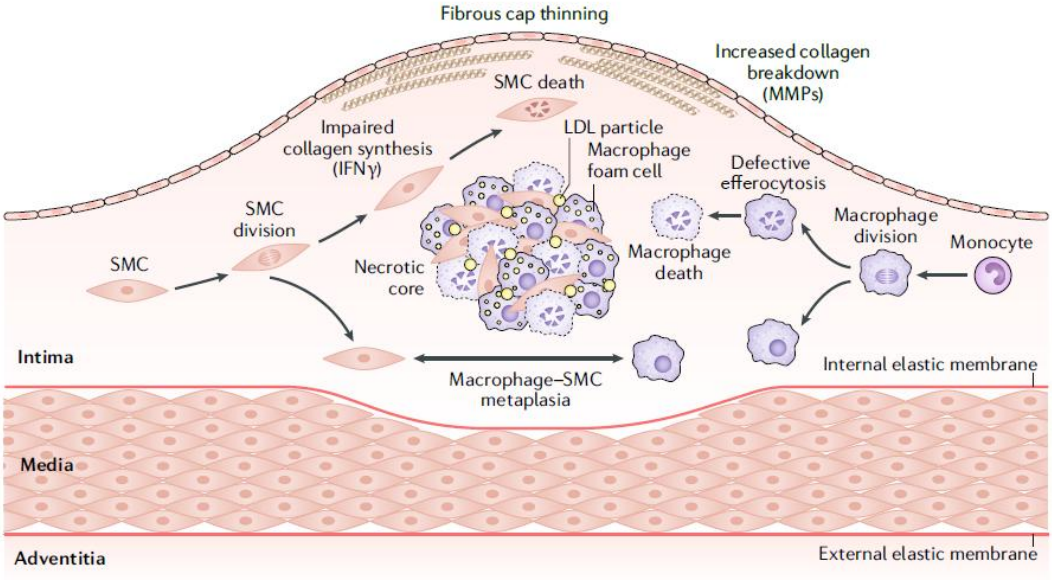


**Figure 4 Progression of atherosclerosis**
A schematic representation of atheroma progression. Depicted is the contribution of both SMCs and macrophages to plaque growth, and their accumulation as dead cells inside the necrotic core.
Source: Libby, P. et al 2019, *Copyright © 2019 Springer Nature Limited*
Reproduced with permission from Springer Nature

Another characteristic of plaque progression is calcification. During this process a calcium deposition inside the plaque occurs[35]. Poorly calcified atheroma tend to be more unstable and have a higher tendency to rupture and are more likely to cause a thrombotic event[36], whereas large quantities of calcium deposits decrease the probability for a thrombotic event[37].

## 3. Complications of atherosclerosis

### 3.1 Plaque rupture

Atherosclerotic lesions become life-threatening when the plaque ruptures and a local thrombus that occludes the arterial vessel is formed. This is one of the most common events leading to acute myocardial infarction. The susceptibility to plaque rupture depends mostly on the composition of the necrotic core and the fibrous cap covering the plaque. A large necrotic core covered by a thin fibrous cap is considered a vulnerable plaque, whereas a stable plaque contains a small necrotic core covered by a thick fibrous cap[38,39]. Numerous mechanisms, such as shear stress and pro-inflammatory processes can influence plaque vulnerability[40-42]. For example, activated inflammatory cells can secrete different proteolytic collagenases, contributing to the thinning of the fibrous cap and thereby directly facilitating plaque rupture[43]. Moreover, the cholesterol crystals (CCs) present in the necrotic core have been shown to be involved in the activation of inflammatory cells, further promoting plaque rupture by causing traumatic or inflammatory injury[44]. Current therapies for cardiovascular diseases via statins or PCSK9 inhibitors have been observed to increase the stability of the atheroma and reduce the risk of plaque rupture[45].

Nonetheless, acute coronary syndromes can also develop under conditions of stable plaques via a mechanism called plaque erosion. Atheroma that are prone to disruption by erosion tend to have large areas of extracellular matrix, smaller lipid cores and relatively low levels of myeloid cells[46]. Some evidence suggests that neutrophils and their pattern recognition receptors such as Toll-like receptor 2 (TLR-2) contribute to plaque erosion[47,48]. Neutrophils and their neutrophil extracellular traps (NETs) have also been described as propagators of thrombosis when thrombus formation was caused by plaque erosion[47]. Upon vessel occlusion in patients with carotid stenosis, the presence of NETs was associated with an unstable atheroma[49].

### 3.2 Atherothrombosis

#### *3.2.1 The role of fibrin and platelets*

Once the plaque ruptures, its core components, lipids, cholesterol crystals, cell debris, cytokines and especially TF are exposed to the bloodstream and a thrombus starts to build up at the site of the lesion (atherothrombosis)[50]. The thrombus can grow to occlude the vessel lumen and cause an ischaemic condition such as in case of stroke or myocardial infarction, or the vessel occlusion is limited and vessel restitution ensues (Figure 5).

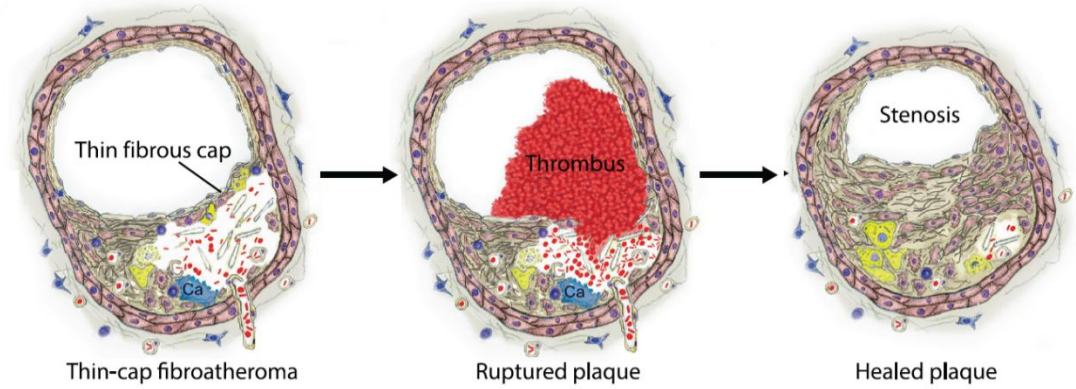


**Figure 5 Plaque induced thrombosis**
A graphical representation of thrombus formation upon plaque rupture and the subsequent vessel restitution.
Source: Bentzon et al. 2014, Copyright © 2014 Wolters Kluwer Health
Reused with Permission from Wolters Kluwer Health

Thrombi that arise from ruptured atherosclerotic plaques promote local fibrin generation, mostly via the TF-initiated extrinsic pathway of coagulation. Furthermore, the rapid aggregation of platelets upon plaque rupture is a major promoter of atherothrombosis. Platelet glycoprotein (GP) Ibα receptor can be anchored to plaque collagen via von Willebrand factor (vWF)[51]. GPIbα also contains a binding site for the leukocyte integrin macrophage-1 antigen (MAC-1) which allows platelets to directly recruit leukocytes to the lesion site[52-54]. Another important platelet receptor is GPVI which also allows platelets to adhere to exposed collagen from the plaque and plays a major role in further propagating platelet activation, vascular inflammation and atheroprogression[55,56]. All these receptors ensure that the thrombus buildup can facilitate vessel occlusion upon plaque rupture.

### 3.2.2 The role of immune cells in Atherothrombosis

Myeloid immune cells are among the first cells recruited to the site of the thrombus buildup upon plaque rupture. In particular neutrophils, which have been described to promote atherothrombosis by secreting NETs[57]. NETs consist of chromatin, granule proteins and enzymes which are produced by neutrophils when they undergo the process of NETosis. The thrombus consisting of NETs, activated platelets and fibrin strands propagates further fibrin formation and amplifies the thrombus formation[58,59].

The role of lymphocytes in the regulation of plaque-induced thrombosis is less clear. The ecto-ATPase present on lymphocytes can convert platelet-released ATP into ADP and thus further enhance platelet aggregation[60]. Platelets also have the ability to form conjugates with lymphocytes[61], helping them to adhere to the lesion site under high shear stress conditions, which in turn further promotes platelet aggregation[62]. Platelets can increase T cell cytokine production via CD154 (CD40L-CD40)[63], and stimulate through cell-to-cell interaction, the clonal expansion of $CD4^+$ T cells. Furthermore, platelets have been observed to enhance Th17 T cell differentiation as well as IL-17 production, a cytokine which affects the ability to recruit neutrophils to the site of the lesion[64]. Also, IFN-γ released by T lymphocytes can increase the secretion of platelet granules and the formation of platelet-lymphocyte complexes and IL-2 has been shown to promote the secretion of platelet α-granules (containing multiple clotting proteins and growth factors)[65,66].

Transforming growth factor beta (TGF-β) released by platelets inside the thrombus can stimulate the SMCs to migrate into the newly formed thrombus and to start producing extracellular matrix. This further stabilizes and contributes to the size of the growing thrombus.

Overall, the involvement of immune cells in the acute phase of arterial thrombosis is under-investigated although arterial thrombi are already known to contain multiple immune cell types. Therefore, it is the aim of this study to examine the effects of the different myeloid and lymphoid cell subtypes on the initial stages of thrombus formation upon plaque rupture.

## II. Objectives of the study

The development of arterial thrombosis in response to the rupture of atherosclerotic plaques is a critical event responsible for the high morbidity and mortality of cardiovascular diseases such as myocardial infarction or stroke. Analysis of arterial thrombi formed upon atherosclerotic plaque rupture has shown considerable amounts of myeloid and lymphoid immune cells. Hence, we have attempted to obtain more insight into the role that some of these immune cells play in plaque-induced thrombosis.

The following questions were addressed:

- Are neutrophils, classical and non-classical monocytes, and T cells, regular components of arterial thrombi recovered from carotid and femoral arteries?
- To what extent do cholesterol crystals (CCs) and homogenised atherosclerotic plaques influence the coagulation process in human whole blood?
- How do classical monocytes and $CD4^+$ T-cells regulate plaque-induced thrombus formation?
- To what extent does PAI-1 affect thrombus formation in the early stages of coagulation?

## III. Materials and methods

1. Materials

### 1.1 Equipment and materials

**Table 3 Equipment and materials**

| | |
|---|---|
| Analysis scale LA 214i | VWR International (Radnor, USA) |
| Axio Zoom Microscope | Zeiss (Oberkochen, Germany) |
| Axiovert 100 light microscope | Carl Zeiss GmbH (Jena, Germany) |
| Bacterial Shaker / Agitation plate Innova 4330 | New Brunswick Scientific (New Jersey USA) |
| Balance MC1 LC 620 S | Sartorius (Göttingen, Germany) |
| Biological safety work bench MSC Advantage | Thermo Fisher Scientific GmbH (Schwerte, Germany) |
| Centrifuge (Rotina 22R, 35R) | Hettich GmbH & Co. KG (Tuttlingen, Germany) |
| Coverslips Ibidi | Ibidi (Gräfelfing, Germany) |
| Eppendorf tubes | MilliporeSigma (Burlington, MA, USA) |
| Falcon Tubes | Corning (NY, USA) |
| Ibidi Sticky slide 0.2 µm – 0.8 µm | Ibidi (Gräfelfing, Germany) |
| Incubator C series | Binder GmbH (Tuttlingen, Germany) |
| Lab Oven | Heraeus (Hanau, Germany) |
| Leica CM3050 Cryostat | Leica Biosystems (Wetzlar, Germany) |
| Leica SP8X WLL confocal microscope (Core Facility Bioimaging, LMU) | Leica Biosystems (Wetzlar, Germany) |
| LSM 510 Meta confocal laser microscope | Carl Zeiss GmbH (Jena, Germany) |
| LSRFortessa™ Cell Analyzer | BD Biosciences (New Jersey, USA) |
| Magnetic stirrer RCT | IKA GmbH & Co. KG (Staufen, Germany) |
| Micropipettes (2.5 µL, 10 µL, 20 µL, 200 µL, 1000 µL) | Eppendorf AG (Hamburg, Germany) |
| Neubauer imroved cell counting chamber | Brand GmbH & Co. KG (Wertheim, Germany) |
| O.C.T. Tissue Tek | Sakura Finetek (Torrance, USA) |
| Percellys Tissue homogenizer | Bertin Instruments (Montigny-le-Bretonneux, France) |
| Perfussor Pump Alaris GH | Cardinal Health (Dublin, Ohio, United States) |
| pH-Meter HI221 | HANNA Instruments (Québec, Canada) |
| Pipette (serol, Wattestopf, 10 ml) | Omnilab GmbH & Co. KG (Bremen, Germany) |
| Pipette (serol, Wattestopf, 5 ml) | Omnilab GmbH & Co. KG (Bremen, Germany) |
| Pipette tips Biosphere Filter Tips 0.1-2.5 µL | Sarstedt AG & Co. (Nümbrecht, Germany) |
| Pipette tips Biosphere Filter Tips 100-1000 µL | Sarstedt AG & Co. (Nümbrecht, Germany) |

| | |
|---|---|
| Pipette tips<br>Biosphere Filter Tips 1-10 µL | Sarstedt AG & Co. (Nümbrecht, Germany) |
| Pipette tips<br>Biosphere Filter Tips 2-200 µL | Sarstedt AG & Co. (Nümbrecht, Germany) |
| Pipettes (5ml, 10ml) | Omnilabs GmbH Co. KG (Bremen, Germany) |
| Plate Reader SpectraMax® Paradigm® | Molecular Devices (San Jose, USA) |
| Polyethylene tube | Smith Medical ASD (Keene, USA) |
| Potter-Elvehjem PTFE<br>pestle and glass tube | MilliporeSigma (Burlington, MA, USA) |
| Pressure pot | WMF (Geislingen an der Steige, Germany) |
| ROTEM® Cup und Pin pro | Tem Innovations GmbH (München, Germany) |
| Safe-Lock reaction vial (0.5 ml, colourless) | Omnilab GmbH & Co. KG (Bremen, Germany) |
| Safe-Lock reaction vial (1.5 ml, colourless) | Omnilab GmbH & Co. KG (Bremen, Germany) |
| Safe-Lock reaction vial (2 ml, colourless) | Omnilab GmbH & Co. KG (Bremen, Germany) |
| Safety-Multifly® Needle 21G | Sarstedt AG & Co. (Nümbrecht, Germany) |
| Sterile filter 0.22 µm | VWR International (Radnor, USA) |
| Superfrost+ microscope slide | Thermo Fisher Scientific Ltd. (Waltham, USA) |
| Syringe (10 ml) | BD Pharmingen (Franklin Lakes, USA) |
| Syringe (5 ml) | BD Pharmingen (Franklin Lakes, USA) |
| Syringe Inject®-F 1 ml | B. Braun (Melsungen, Germany) |
| Thromboelastograph ROTEG® 05 | Pentapharm GmbH (Munich, Germany) |
| TissueTek Cryomold | Sakura Finetek (Torrance, USA) |
| Vortex Genie 2 | Scientific Industries Inc. (Bohemia, NY, USA) |
| Vortexer | Sartorius (Göttingen, Germany) |
| Water Bath Julabo U3 | Julabo Labortechnik GmbH (Allentown, USA) |

## 1.2 Reagents and chemicals

**Table 4 Reagents and chemicals**

| Substance | Manufacturer | Product ID |
|---|---|---|
| Alexa Fluor 488 Conjugation Kit | Abcam plc (Cambridge, UK) | ab236553 |
| Anilin blue solution | Electron Microscopy Sciences (Hatfield, USA) | 26381-06 |
| Beriplex® P/N | CSL Behring, (Marburg, Germany) | / |
| Bovine serum albumin (heat shock fraction; pH 7; 98 %) | Sigma-Aldrich GmbH (Hamburg, Germany) | A7906-100G |
| Calcium chloride dihydrate 99% | Carl Roth GmbH & Co. KG (Karlsruhe, Germany) | HN04.1 |
| Chlorampenicol | Sigma-Aldrich GmbH, (Steinheim, Germany) | C0378-25G |
| Chromogenic Substrate S-2222 | Haemochrom Diagnostica (Essen, Germany) | 41201 |
| Corn trypsin Inhibitor (CTI) | Haematologic Technologies Inc. (Essex Junction, USA) | CTI-01 |
| Covering solution with DAPI | Abcam (Cambridge, UK) | ab104139 |
| DAPI | Sigma-Aldrich GmbH (Hamburg, Germany) | D9564 |
| Dextrose | Thermo-Fisher Scientific, (Carlsbad, USA) | D16-1 |
| Disodium hydrogen phosphate - dihydrate 99.5% | Carl Roth GmbH & Co. KG (Karlsruhe, Germany) | 4984.1 |
| DMEM, high glucose, L-glutamine, no sodium pyruvate, no phenol red | R&D Systems (Minneapolis, USA) | M12950 |
| DMSO | PAN Biotech GmbH (Aidenbach, Germany) | P60-36720100 |
| DRAQ5 | Thermo Fisher Scientific Ltd. (Waltham, USA) | 62251 |
| Dulbecco's Modified Eagle Medium (4.5 g/L) | Thermo Fisher Scientific Ltd. (Waltham, USA) | 41965-039 |
| EDTA | Sigma-Aldrich GmbH (Hamburg, Germany) | E-9884 |
| Eosin G | Carl Roth GmbH & Co. KG (Karlsruhe, Germany) | 7089.1 |
| Ethanol | Carl Roth GmbH & Co. KG (Karlsruhe, Germany) | K928.4 |

| | | |
|---|---|---|
| Factor XII deficient plasma | Haematologic Technologies Inc. (Essex Junction, USA) | FXII-ID-1 |
| Fetal bovine serum (FBS) | Thermo Fisher Scientific Ltd. (Waltham, USA) | 10270106 |
| Fibrinogen from human plasma | Sigma-Aldrich GmbH (Hamburg, Germany) | F3879 |
| Ficoll-Paque PREMIUM | Cytiva Sweden AB (Uppsala, Sweden) | 17544202 |
| Filipin complex | Sigma-Aldrich GmbH (Hamburg, Germany) | SAE008 |
| FM™ 4-64 Stain | Thermo Fisher Scientific Ltd. (Waltham, USA) | **T3166** |
| Formaline | Sigma-Aldrich GmbH (Hamburg, Germany) | F-8775 |
| Glycerol | Merck (Darmstadt, Germany) | 356350-1000ML |
| Goat serum | Sigma-Aldrich GmbH (Hamburg, Germany) | G6767 |
| Hepes 99% | Carl Roth GmbH & Co. KG (Karlsruhe, Germany) | 9105.4 |
| Hoechst 33342 | ImmunoChemistry Technologies, (Bloomington, USA) | 639 |
| Hydrochloric acid 37% reconstituted | Carl Roth GmbH & Co. KG (Karlsruhe, Germany) | 9277.1 |
| Ferric-ammoniumsulfate solution (5% water) | Electron Microscopy Sciences (Hatfield, USA) | 26381-01 |
| Mayer's Hämatoxylin | Electron Microscopy Sciences (Hatfield, USA) | 26381-02 |
| Paraformaldehyde | Sigma-Aldrich GmbH (Hamburg, Germany) | P6148.500G |
| PBS (Dulbecco's Phosphate Buffered Saline) | Sigma-Aldrich Chemie GmbH (Steinheim, Germany) | D-8537-500ML |
| Phosphotungstic acid 1% | Electron Microscopy Sciences (Hatfield, USA) | 26381-05 |
| Picric acid -Orange G solution | Electron Microscopy Sciences (Hatfield, USA) | 26381-03 |
| Ponceau Fuchsin- Solution | Electron Microscopy Sciences (Hatfield, USA) | 26381-04 |
| Potassium chloride | Merck KGaA (Darmstadt, Germany) | 4936 |
| Potassium hydrogen phosphate | Carl Roth GmbH & Co. KG (Karlsruhe, Germany) | 3904.1 |
| RBC Lysis Buffer 10x | Invitrogen eBioscience (Waltham, USA) | 00-4300-54 |

| | | |
|---|---|---|
| Roti-Mount | Carl Roth GmbH & Co. KG (Karlsruhe, Germany) | HP68.1 |
| Sodium chloride 99% | Carl Roth GmbH & Co. KG (Karlsruhe, Germany) | P029.2 |
| Sodium hydroxide solution min. 32% | Merck KGaA (Darmstadt, Germany) | 5590 |
| Substrate S-2251 | Haemochrom Diagnostica (Essen, Germany) | 41206 |
| Tris | Carl Roth GmbH & Co. KG (Karlsruhe, Germany) | 5429.3 |
| Trisodium Citrate dihydrate | Merck KGaA (Darmstadt, Germany) | 1.12005 |
| Trypsin-EDTA solution 10x | Sigma-Aldrich GmbH (Hamburg, Germany) | 59418C |
| Tryptan blue | Carl Roth GmbH & Co. KG (Karlsruhe, Germany) | CN76.1 |
| Tween20 (Polyoxethylene) | Sigma-Aldrich GmbH (Hamburg, Germany) | P1379 |
| Xylene | Honeywell Intternational Inc. (Muskegon, USA) | 247642 |
| Zelltracker CellTracker™ Red CMTPX | Thermo Fisher Scientific Ltd. (Waltham, USA) | C34552 |
| Zelltracker CytoTrace™ Red CMTPX | AAT Bioquest Inc. (Sunnyvale, USA) | 22015 |

## 1.3 Antibodies

**Table 5 Antibodies used in Immunohistochemistry**

| Antibody against | Conjugation | Concentration IHC staining | Host | Reactivity | Firm Product Number |
|---|---|---|---|---|---|
| CD3 | / | 1:100 | Rabbit | Human, Mouse, Rat | Novusbio NBP1-72186 |
| CD4 | / | 1:100 | Mouse | Human | Sino Biological 10400-MM23 |
| CD14 | / | 1:100 | Rabbit | Human | Sino Biological 10073-R001 |
| CD16 | / | 1:250 | Mouse | Human | Sino Biological 10389-MM04 |
| CD41 | / | 1:50 | Rabbit | Mouse, Human | Abcam Ab63983 |
| MPO | / | 1:25 | Rabbit | Human | Abcam ab9535 |
| Anti-Histone H3 | / | 1:200 | Rabbit | Human, Mouse, Rat | Abcam Ab5103 |
| tPA | / | 1:200 | Rabbit | Human, Mouse, Rat | Proteintech 10147-1-AP |
| uPAR | / | 1:100 | Rabbit | Human, Mouse | Proteintech 10286-1-AP |
| uPA | / | 1:100 | Rabbit | Human, Mouse, Rat | Proteintech 17968-1-AP |
| ROR-γ-T | / | 1:50 | Mouse | Human | Millipore MABF81 |

## 1.4 Buffers

**Table 6 Buffers**

| Buffer | Ingredients |
|---|---|
| Blocking buffer | 1.5g BSA<br>100 ml ddH2O |
| Buffer B (Plasmin activity assay) | 40mM TrisHCL (Tris adjusted to 7.2-7.4 pH with HCL)<br>75 mM $CaCl_2$<br>0.01% Twwen-20 |
| Buffer C (plasmin activity assay) | Buffer B + 1mg/ml BSA |
| Buffer for heat-induced antigen retrieval – Sodium citrate Tween20 | Sodium citrate 10mM<br>0.05% Tween 20<br>pH 6.0 |
| $Ca^{2+/}$Hepes | 10 mM Hepes<br>100 mM $CaCl_2$<br>ddH2O, pH 7.4 |
| Dialysis buffer for plaque homogenisation | NaCl 150mM<br>EDTA 1mM<br>Chlorampenicol 0.05% (w/v) |
| HEPES buffer | NaCl 140 mM<br>KCL 2.7mM<br>HEPES 3.8 mM<br>EGTA 5 mM<br>pH 7.4 |
| MACS buffer & FACS buffer | PBS<br>0.5% Bovine serum albumin<br>EDTA 2 mM |
| PBS (Phosphate Buffered Saline) (1L) | 8 g NaCl<br>0.2 g KH2PO4<br>1.42 g Na2HPO4.2H2O<br>0.2 g KCl<br>ddH2O |
| RBC Lysis buffer 1x | 8.26g Ammoniumchloride<br>1g Potassiumhydrogencarbonate<br>100 µL 0.5 M EDTA (pH 8)<br>1 Litre distilled water |
| TBS Tween20 | For 1 L: 100 ml of TBS 10x + 900 ml ultra-pure water + 1 ml Tween20 |
| TNC (Trisodium citrate) | 3.68 g TNC<br>100 ml ddH2O |
| Tris-buffered saline 10x (concentrated TBS) | 24.23 g Trizma HCl<br>80.06 g NaCl<br>Mix in 800 ml ultra-pure water.<br>pH to 7.6 with pure HCl.<br>Top up to 1 L |

## 1.5 Antibody and Isolation kits

**Table 7 Antibody/Isolation kits**

| Name | Firm |
|---|---|
| Lightning-Link®Rapid Alexa Fluor® 555 | Abcam |
| Lightning-Link®Rapid FITC | Abcam |
| AbSelect™ Antibody Concentration kit | Abcam |
| MiniMACS™ Starting Kit | Miltenyi Biotec |
| MidiMACS™ Starting Kit | Miltenyi Biotec |
| $CD4^+$ T Cell Isolation Kit, human | Miltenyi Biotec |
| $CD16^+$ Monocyte Isolation Kit, human | Miltenyi Biotec |

## 1.6 Human Tissue samples

**Table 8 Human Tissue Samples**

| Type | Source |
|---|---|
| Carotid and Femoral PAD vessel samples | Munich Vascular Biobank – TUM Rechts der Isar |
| Carotid and Femoral PAD plaque samples | |
| Carotid and Femoral PAD thrombi samples | |

## 1.7 Mouse Models

**Table 9 Mouse models**

| **Type/Name** | **Source** |
|---|---|
| Wild type C57BL/6 | Walter-Brendel-Centre, Munich, GE |
| $F12^{-/-}$ C57BL/6 | Walter-Brendel-Centre, Munich, GE |

# 2. Methods

## 2.1 Blood Drawing

Blood was collected from healthy volunteers (aged 18-65, with a ratio of approx. 50/50 male/female), who denied having taken anticoagulants or anti-platelet drugs in the past 14 days. All volunteers were in a fasting state.

Prior to drawing blood, the skin was disinfected with Cutasept® F for at least 30 seconds, afterwards, the vein was occluded with the help of a tourniquet and blood was drawn into 5 ml – 20 ml syringes (depending on the experiment). A butterfly needle catheter (21G) was used to draw the blood. After that, it was ensured that the bleeding has stopped, before releasing the volunteers.

To collect blood for TEG measurement, 5 ml syringes were used. The syringes were filled beforehand with Trisodium Citrate (TNC) 500 µL per 5 ml and corn trypsin inhibitor (CTI) 5 µg/ml to prevent blood coagulation by the artificial surface of the wall of the syringes. For the blood samples which were used in cell isolation or plasma separation only TNC was used.

## 2.2 Preparation and treatment of Human Whole Blood – Cell isolation

Two different methods were used to obtain a single cell suspension of mononuclear cells from fresh human blood. The method used depends on the requirements of the different experimental setups.

### 2.2.1 Isolation of mononuclear cells from human peripheral blood by density gradient centrifugation or red blood cell (RBC) lysis

PBMCs were isolated from fresh human blood via density gradient centrifugation. The freshly drawn blood was first diluted 2-4 times with PBS (2mM EDTA) buffer. 35 ml of diluted blood was layered over 15 ml of Ficoll-Paque in a 50 ml Falcon tube. Attention was given not to mix the two layers to achieve clear separation. The sample was then centrifuged at 400 x g for 35 min. Afterwards 2/3 of the upper plasma layer was aspirated, leaving the PBMCs at the interphase undisturbed (Figure 6).

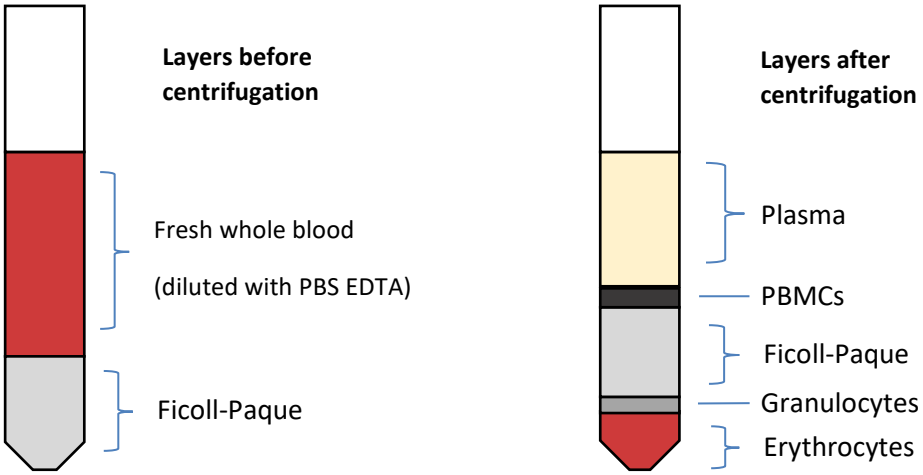


**Figure 6 Density gradient centrifugation with Ficoll-Paque**
A schematic representation of the different layers visible before and after density gradient centrifugation with Ficoll-Paque.

The cells of the interphase were collected with a Pasteur pipette, resuspended in PBS-EDTA buffer, and then centrifuged at 300 x g for 10 min at room temperature (RT). For the removal of thrombocytes, the suspension was centrifuged at 200 x g for 10-15 min at RT after which the supernatant was removed completely.

This step was repeated twice to increase the purity of the cell suspension and to make sure all thrombocytes had been removed. The pellet containing the PBMCs was then transferred to an Eppendorf tube for further use.

**Red blood cell (RBC) lysis**

For the extraction of a PBMC suspension from fresh whole blood. 1 ml of 1x RBC Lysis Buffer was added to 10 ml of fresh human whole blood. The mixture was then incubated for 10 min at RT and afterwards, the reaction was stopped by adding 20 ml of PBS. Afterwards the mixture was centrifuged at 300 x g for 10 min. at 2-8ºC to pellet all the cells. Because the erythrocytes had been lysed, they could not sediment to the bottom of the falcon tube. In the next step, the supernatant (red blood cells and buffer) was aspirated with a Pasteur pipette and discarded, while being careful not to disturb the cell pellet.

To increase the purity and to obtain an RBC-free pellet the above steps including incubation, centrifugation and removal of supernatant were repeated once.

The pellet containing the PBMCs was then resuspended in the appropriate buffer for use in further experiments.

### 2.2.2 Preparation of platelet rich plasma (PRP) and platelet poor plasma (PPP) from human whole blood

Fresh whole blood from volunteers, anticoagulated with TNC was used for the preparation of platelet-rich and platelet-poor plasma. The blood sample was centrifuged at 200 x g in a centrifuge tube for 20 min to achieve layer separation yielding PRP. At this step, the PRP can be aspirated with a Pasteur pipette, and after being recalcified with $Ca^{2+}$ /Hepes, be further used in experiments.

The PRP was centrifuged at 800 x g for 20 min to pellet the thrombocytes and yield PPP. The layer of PPP was aspirated using a Pasteur pipette and portioned into Eppendorf tubes for further use.

### 2.2.3 Isolation of classical monocytes using magnetic-activated cell sorting (MACS)

To obtain a single cell suspension of classical human monocytes from fresh human whole blood, a MACS kit from Miltenyi Biotec was used. PBMCs were isolated using density gradient centrifugation (2.2.1) and the obtained pellet was resuspended in MACS buffer.

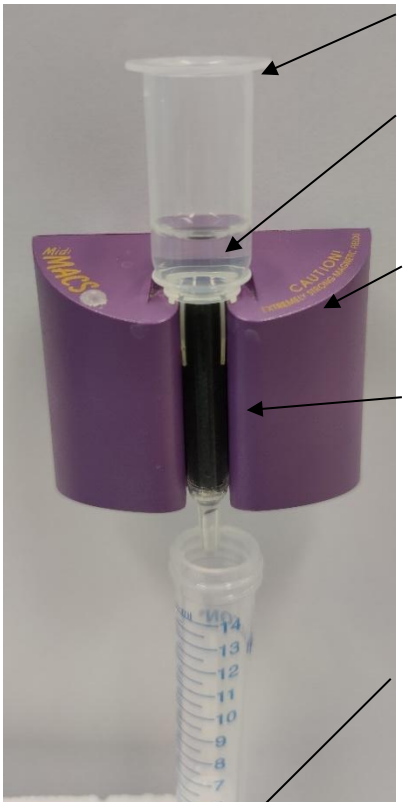


**Figure 7 Representation of the MACS system in use**

For the MACS isolation, a MidiMACS Separator magnet, anti-CD14 microbeads and LS columns were used (Figure 7).

PBMCs ($10^7$ cells) were resuspended in 80 µL MACS Buffer. Afterwards 20 µL of anti-CD14 microbeads were added, the sample was mixed and incubated for 15 min at 4°C. The cells were then washed with 1.5 ml of MACS buffer and centrifuged at 300 x g for 10 min. The pellet was then resuspended in 500 µL MACS buffer.

An LS Column was then placed in the MidiMACS magnet and washed with 3 ml of MACS buffer. This effluent was discarded. The cell suspension was applied onto the column and washed afterwards three times with 3 ml of MACS buffer to make sure that the unlabelled cells had been washed out of the column. The labelled cells remained inside the column. The effluent represents the fraction of all unlabelled cells and could be either discarded or used in further experiments. The column was then removed from the separator, and by using the plunger provided with the column, the labelled cell fraction was washed out with 5 ml of MACS buffer. The suspension was centrifuged at 300 x g for 10 min and the pellet was ready to be used.

### 2.2.4 Isolation of non-classical human monocytes using MACS

For the isolation of non-classical monocytes with MACS, a MidiMACS separator, $CD16^+$ Monocyte kit, an LD Column and an LS Column were used.

PBMCs ($10^8$ cells) isolated with Ficoll-Paque separation were resuspended in 300 µL of MACS buffer. The suspension was then incubated with 100 µL of FcR Blocking Reagent (provided in the kit) and 100 µL non-Monocyte depletion cocktail (provided in the kit) for 15 min in a 4°C refrigerator. Afterwards the cells were washed with 5 ml of MACS buffer and centrifuged at 300 x g for 10 min.

The LD column was rinsed with 2 ml of MACS buffer. Then, the pellet was resuspended in 500 µL MACS buffer and applied onto the LD column (using the plunger provided in the kit). The unlabelled cells which had passed through the column were collected and the column was washed with another 2 ml of MACS buffer. The cell suspension collected represented the pre-enriched $CD16^+$ monocyte cell fraction.

The cells were pelleted again (300 x g for 10 min RT) and then resuspended in 400 µL of MACS buffer. 100 µL of anti-CD16 Microbeads were added and the suspension was incubated for 15 min in a 4°C refrigerator. The cells were again washed and pelleted before being resuspended in 500 µL of MACS buffer. A LS-Column was prepared by washing the column with 3 ml of MACS buffer. The cell suspension was then applied onto the column and the unlabelled cell fraction was collected. The column was washed three times with 3 ml MACS buffer to ensure purity of the cell fraction inside the column. The total effluent represented the unlabelled cells. The $CD16^+$ monocyte fraction was flushed out by removing the column from the magnet and applying 5 ml of MACS buffer onto the column by pressing firmly with the plunger.

### 2.2.5 Isolation of human $CD4^+$ T helper Cells using MACS

For the isolation of $CD4^+$ T helper cells with MACS, a MidiMACS magnet, CD4+ T Cell Isolation kit and a LS column were used.

PBMCs ($10^7$ cells) isolated from human whole blood, were resuspended in 40 µL of MACS buffer. Afterwards 10 µL of $CD4^+$ T Cell Biotin-Antibody Cocktail was added, and the suspension was incubated for 5 min in a 4°C refrigerator. Then 30 µL of MACS buffer and 20 µL of anti-$CD4^+$ T Cell Microbead Cocktail was added. The suspension was incubated for 10 min in a 4°C refrigerator.

A LS Column was rinsed with 3 ml of MACS buffer. The cell suspension was then applied onto the column using the plunger. Afterwards the column was washed with 3ml of MACS buffer. The total effluent (the unlabelled cells which had been passed through) represent the enriched $CD4^+$ T cells.

The cells were then washed and pelleted to be counted or used in further experiments.

### 2.2.6 Cell number determination

The cell number was determined using a light microscope with 10x magnification and an improved Neubauer cell counting chamber. A new suspension was prepared which consisted of 40 µL PBS, 5 µL Trypan Blue stain and 5 µL of the cell suspension, containing the cells of interest. In the counting chamber, all the cells in the four outer fields and the centre were counted.

The following formula was used to calculate the cell number per 1 µL of cell suspension:
Cell Count/µL = (Chamber 1st side + 2nd side)/2 x 50 x Dilution Factor

Dilution factor was equal to 10.

## 2.3 Preparation and treatment of Mouse Whole Blood

All mouse blood samples were provided by a cooperation group. The samples were taken directly via heart puncture with a syringe containing TNC by qualified laboratory assistant in accordance with the lab's protocols. The samples were directly used for ROTEM measurement after being diluted 1:1 with PBS.

## 2.4 Activation of isolated classical monocytes with lipopolysaccharide (LPS)

LPS was used for the activation of the isolated classical monocytes. The isolated cell pellet was reconstituted in PBS and then LPS was added at 500 ng/ml. The cells were incubated in a falcon tube inside a cell incubator (37°C, 5.0% $CO_2$) for 4 h. After that, the cells were pelleted and washed twice before being resuspended for further use.

## 2.5 Activation of isolated non-classical monocytes with oligoribonucleotides (ORN)

For the activation of non-classical monocytes, the ORN-0006 kit from Miltenyi Biotec, as well as the recommended activation protocol in the product data sheet was used.

Oligoribonucleotides (ORN), a TLR7/TLR8 agonist, were used for the activation of the isolated non-classical monocytes. Lyophilized ORN (Miltenyi Biotec), DOTAP-Chloride (Miltenyi Biotec) and RNase-free water were used. Aliquots of 200 µM ORN (200 µg lyophilized ORN as provided in the kit, resuspended in 151 µL of RNase-free Water) were prepared and stored in a -20°C freezer. Before the activation step, a 2 µM ORN solution (2 µL 20 µM ORN + 8 µL RNase-free Water) and a 25 µg/ml DOTAP-Chloride solution (5 µL RNase-free Water + 5 µL DOTAP-Chloride) were prepared.

The diluted DOTAP was added to the diluted ORN, and the resulting suspension was then applied to the cells. 20 µL of ORN/DOTAP-Cl complex was added to $10^6$ non-classical monocytes (isolated via MACS). The cells were then put in an incubator (37°C, 5.0% $CO_2$) for 4 h before being used in further experiments.

## 2.6 Homogenisation of human carotid plaque tissues

Human plaque tissue was stored at -80°C frozen in DMSO or PBS. After thawing of the tissue samples, any thrombus material (identified by its colour, form, and consistency) was mechanically removed using a scalpel (Figure 8). The rest of the tissue (altered vessel wall with plaque build-up) was weighed. 100 mg of plaque tissue was then added to 1 ml of dialysis buffer at a concentration of 100 mg/ml[67].

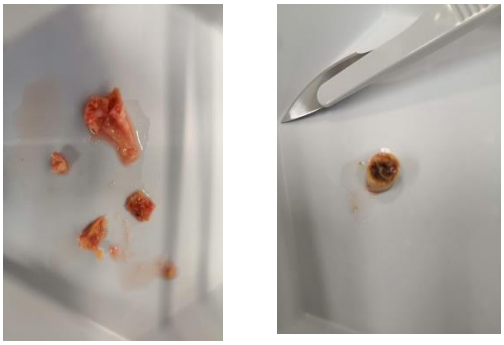

**Figure 8 Carotid tissue samples**
The darker coloured tissue represents the thrombus inside the vessel lumen. The light outer part, the vessel wall, and the atheroma.

The tissues were then homogenised in dialysis buffer with a Potter-Elvehjem PTFE pestle in a glass tube for approx. 5 min. Then the homogenised plaque material was aliquoted and stored at -80°C until further use (Figure 9).

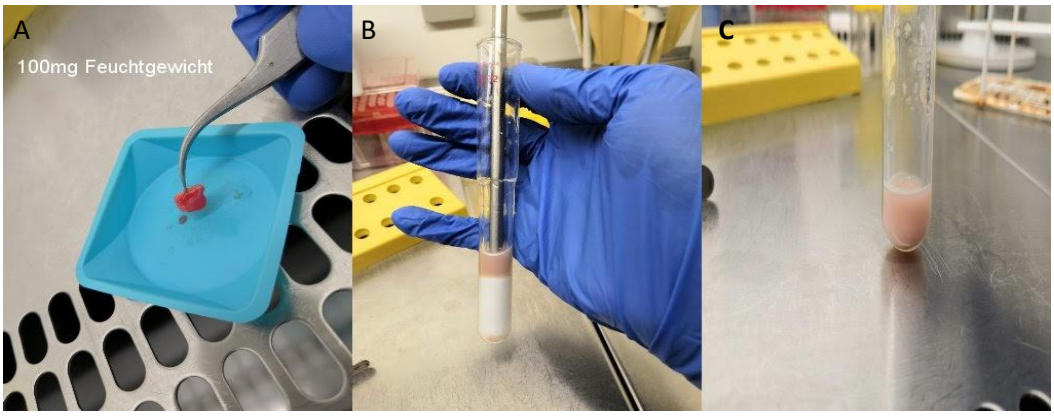


**Figure 9 Homogenisation of plaque samples**
(A) Weighing the material.
(B) Manual homogenisation with pestle in a glass tube with dialysis buffer.
(C) Homogenised plaque in buffer.

## 2.7 Activation of human $CD4^+$ T-cells

For the activation of $CD4^+$ T-cells a combination of anti-CD3 and anti-CD28 antibodies was used. The following protocol was used: A 96-well plate was coated with Poly-L-ornithin and left for 1 h at RT. After that, the plate was washed twice with PBS, coated with anti-CD3 antibody (2 µg/ml), and incubated for 2 h at 37°C. After that, the anti-CD3 solution was discarded. The plate was now ready for the cell suspension. The cells were incubated in the prepared plate with anti-CD28 antibody (20 µg/ml CD28.2, Biolegend) in phenol red free RPMI(Gibco) + glutaMAX Cell medium at 37°C in 5% $CO_2$ for 18-24 h. After 3 h the cell medium was supplemented with 10% foetal calf serum (FBS) to ensure adequate T-cells activation. After that, the cells were harvested and pelleted for further use.

## 2.8 Preparation of cholesterol crystal suspension

To prepare cholesterol crystals, a 2 mg/ml cholesterol solution in 1-propanol was supplemented with 1.5 times the volume of LPS-free ultra-pure water. The solution was then left to dry and crystallise overnight in a lab oven at approximately 30°C.

The crystals were then resuspended in PBS containing 1% BSA at a concentration of 10 mg/ml. Aliquots of the solution were added to Eppendorf tubes with plastic balls of 500 µL and shaken twice with the Percellys 24 tissue homogeniser at a rate of 6000 cycles per min, for 30s each. Afterwards the crystal suspension was tested against calibration beads on the FACS device. The results indicated that the crystals had a size of 3-7 µm and that their average concentration was 3-4 x $10^6$ crystals/µL. All test samples containing cholesterol crystals used in this thesis had these characteristics (Figure 10).

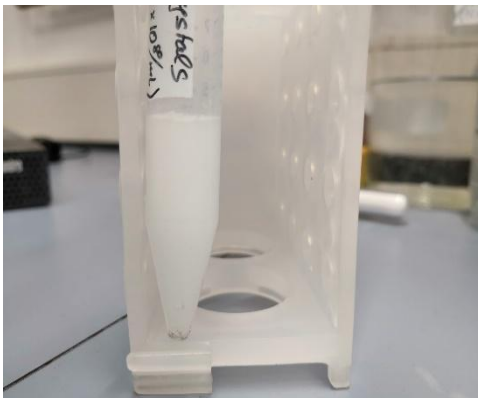

**Figure 10 Cholesterol Crystal Suspension**

## 2.9 Thromboelastography (TEG)

The TEG measurement was carried out in a rotational thromboelastometry device – ROTEM (Figure 11).

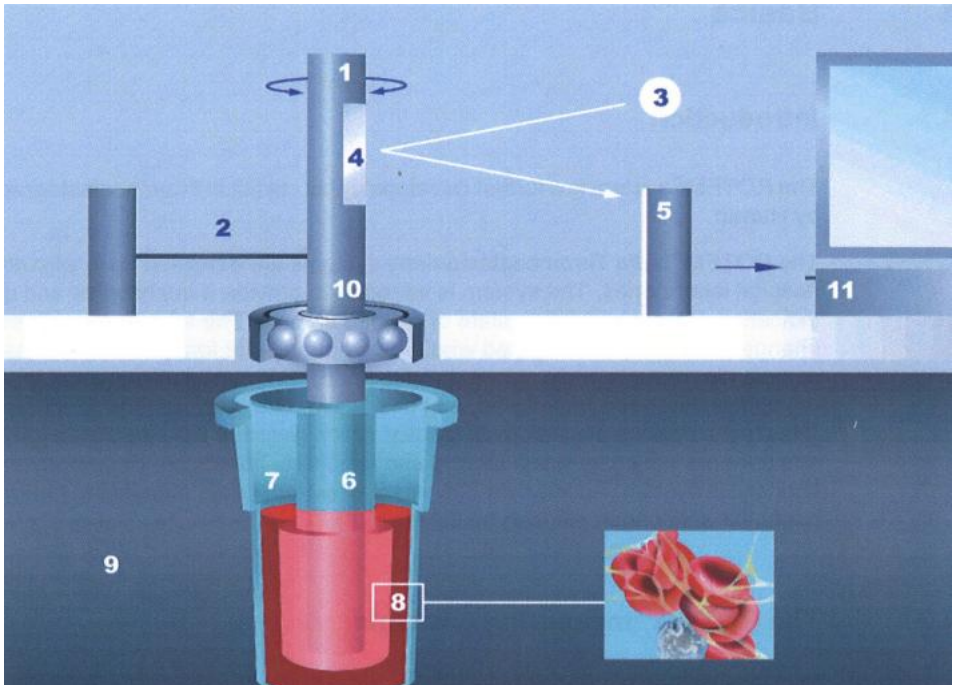


**Figure 11 Principle of function - ROTEM**

1 Axis (≈4.75°)
2 Spring
3 Light source/diode
4 Mirror
5 Detection device
6 Sensor pin
7 Cup filled with blood
8 Fibrin fibres and thrombocyte aggregate
9 Heated cup holder
10 Ball bearings
11 Data processing

Source: Werfen GmbH, used with Permission from Werfen GmbH

The following protocol served as the basis for ROTEM experiments in this thesis and was adjusted where needed according to the experimental setups.

Blood, from a healthy donor (see III.2.1), was drawn into a syringe that contained apart from TNC, also CTI (5 µg/ml) as to prevent unnecessary activation of the intrinsic coagulation pathway. For the isolation of plasma from whole blood only TNC was used, and the blood was directly processed in a centrifuge (see III.2.2.2).

The TEG cup was filled with 270 µL blood/plasma. The mouse whole blood was diluted 1:1 with PBS before being added to the TEG cups. The blood or plasma was slowly pipetted on the wall near the bottom of the cup as to avoid any air bubbles which would distort the measurement.

Afterwards 30 µL of the test sample was added, containing for example either homogenised plaque material or cells of interest. The coagulation was started by adding 60 µL of a $Ca^{2+}$/Hepes solution (100 mM $CaCl_2$, 10 mM Hepes).

The cup was then promptly inserted onto the pin attached on the TEG device and the measurement was started without delay.

When fibrin fibres start to develop, the movement of the pin is obstructed. The computer then detects and measures the difference in the movements of the pin, compared to the beginning of the experiment. By using those data, a graphic is produced which shows the beginning of the measurement, the onset of clotting and clot formation and several additional parameters (Figure 12).

All samples were run in duplicates, 2 channels were used for the control group and 2 other channels for the test sample.

All control measurements for blood and plasma were carried out with 30 µL Dulbecco's modified PBS (without $MgCl_2$ or $CaCl_2$).

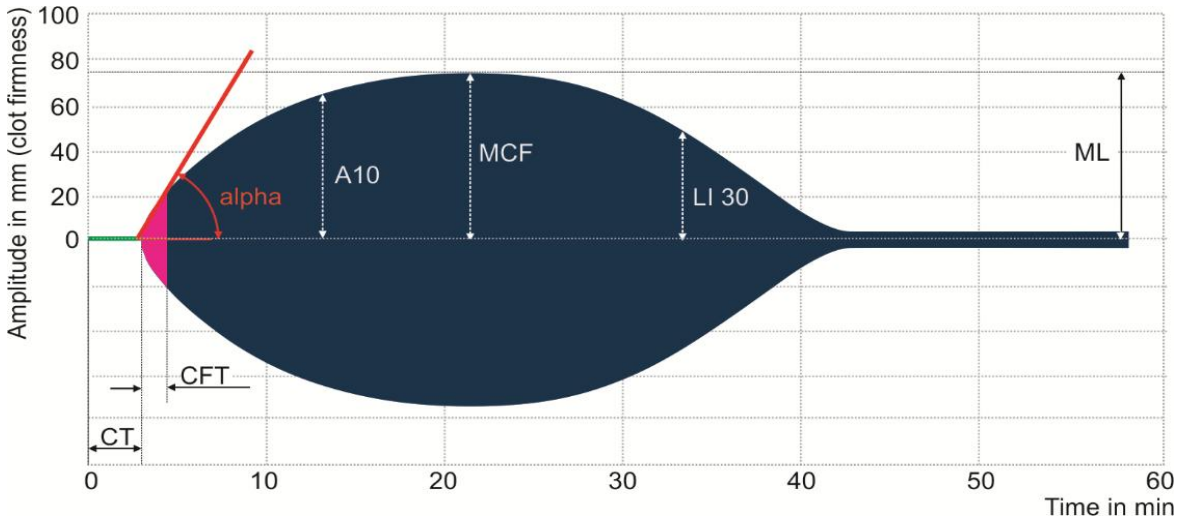


**Figure 12 Graphical representation of the different major ROTEM parameters**
CT (coagulation time) – time until achieving an amplitude of 2 mm
CFT (clot formation time) – time between amplitudes 2 mm and 20 mm
CFR (clot formation rate) – the rate of clot formation - the angle between the baseline and the tangent at the maximum slope
Alpha angle – the angle between the middle axis and the tangent to the clotting curve through the 2 mm amplitude point. It describes the kinetic of clotting.
MCF (maximum clot firmness) – maximum amplitude achieved.
MAXV – maximum velocity to the widest point of the amplitude
ML (maximum lysis) – maximum % clot firmness lost from MCF during the test
TPI- Thrombodynamic Potential Index (<6 represents a hypo coagulative state, >7.5 - a hypercoagulable state.)

Source: Werfen GmbH, used with Permission from Werfen GmbH

### *2.9.1 TEG with cholesterol crystals, homogenised plaque material and immune cells*

Before adding the cholesterol crystal suspension to the blood (or plasma), the suspension was vortexed for at least 30 seconds and promptly pipetted into the cup. Similarly, the homogenised plaque samples, were vortexed for at least 1 min before addition to the cup. For the addition of immune cells, the cells were resuspended in 30 µL of PBS and carefully mixed.

## 2.10 Immunohistochemistry (IHC)

### *2.10.1 Fluorescent IHC staining of frozen sections.*

The tissue samples obtained from femoral or carotid arteries were stored at -80°C before being used for staining. The fresh frozen samples were then embedded in Tissue Tek and cut with a Leica Cryotome at a thickness of 10 µm at a temperature of -20°C. The sections were collected on SuperFrost Plus™ slides.

The sections were then fixed in 4% PFA for 10 min at RT and washed 3 x 3 min with PBS. Afterwards, the slides were placed in a rack and submerged in a blocking solution

(0.1% Triton-X / 1.5% BSA / PBS) for 40 min at RT and then washed with PBS 2 x 5 min.

The unlabelled primary antibody (see Table 5 III.1.3), diluted in PBS, was applied directly to the sections. A DAKO pen was used to prevent the antibody from spilling over the edge of the sections. The slides then were left to incubate overnight at 4°C, for approximately 12-16 h.

On the second day, after washing 2 x 5 min, the slides were incubated with a secondary fluorescent antibody. All fluorescent secondary antibodies were used at a concentration of 1:1000 diluted in PBS or TBS and were chosen to react to the host of the primary antibody. Separately, a blank slide with no primary antibody was stained only with a secondary fluorescent control as a control staining. Afterwards, the slides were mounted with glycerol and a cover glass.

### *2.10.2 Fluorescent IHC staining of paraffin sections.*

All paraffin tissue samples, provided to us by our cooperation, were fixed and embedded in paraffin as per standard protocols used at the Munich Vascular Databank - TUM.

The paraffin blocks were cut with a microtome at a thickness of 5-10 µm and the slides were then floated in a water bath at 30-40°C and picked up on SuperFrost Plus™ slides. The slides were dried in an oven overnight at 37°C and stored in a box at RT until further use.

For the deparaffinization, the slides were washed with the following reagents in this specific order:

Xylene 2 sets each 2 x 3 min.

Xylene 1:1 with 100% ethanol for 3 min

100% ethanol for 2 x 3 min.

95% ethanol for 3 min.

70 % ethanol for 3 min.

50 % ethanol for 3 min.

At the end, the slides were rinsed with cold tap water until the heat-induced antigen retrieval was started.

For the antigen-retrieval, a pressure cooker was filled with Na citrate Buffer (10 mM Na citrate, 0.05% Tween 20, pH 6.0). The slides were heated to above 100°C for 4 min after the pressure cooker reached its full pressure (as indicated by the manufacturer). The pressure cooker was then placed under cold water to depressurize, and then cold water was run through it for 5-10 min to cool down the slides and allow for reconstitution of antigen binding sites.

The slides were then washed 2 x 5 min with a TBS Buffer (see III.1.4) + 0.025% Triton X solution (TBST) with gentle agitation (on a plate shaker at low setting).

For the next step, a blocking solution was prepared (10% FBS, 1% BSA, TBS) and the slides were placed in a rack to block for 2 h at RT.

After this step, the slides were ready for the application of the primary antibody diluted in TBS 1% BSA and left overnight at 4°C.

On the next day, after washing the slides 2 x 5 min in TBST with gentle agitation, the secondary antibody diluted in TBS with 0.1% BSA was applied for 1 hour at RT.

For the last step, the slides were rinsed 3 x 5 min with TBS and then covered with mounting medium and mounted with a coverslip.

#### *2.10.3 Staining of in-vitro cells for Plaque Uptake Experiment*

The cells for the in-vitro plaque uptake experiment (see IV.4.) were stained with a lipophilic stain FM™ 4-64 according to the manufacturer's protocol. The cells were then rinsed and prepared for use and incubation with plaque material in a PBS medium in culture dishes.

### 2.11 Histology

#### *2.11.1 Haematoxylin Eosin (HE) Staining*

The slides with the tissue sections were first deparaffinised in 3 sets of Xylene, each for 10 min. Subsequently the tissues were submerged in descending alcohol concentrations (each for 5 min): 100%, 100%, 95%, 70% and lastly 50% ethanol. Then the sections were washed for 5 min in a PBS solution.

After that, the sections were stained for 20 s with Haematoxylin (after Mayer and Roth). The sections were washed with tap water for 2 min and then stained for 4 min with Eosin. Afterwards, they were washed in distilled water for 1 min.

The sections were dehydrated in consecutive 30 s washes using 50%, 70%, 95% and 2 x 100% ethanol. Afterwards 3 x 5 min washes with Xylene were carried out and then the slides were mounted with cover glasses using glycerol.

### *2.11.2 Carstairs' staining*

For the Carstairs' staining, the paraffin sections were cut at a thickness of 5 µm for optimal staining.

The following steps were carried out:

1. Hydration to distilled water through a series of alcohol solutions with descending concentrations (see III.2.11.1).
2. Soaking of the slides in Ferric Ammonium Sulfate 5% for 5 min and rinsing in tap water
3. Staining with Mayer Hematoxylin for 5 min and rinsing with tap water
4. Staining with Picric Acid-Orange G Solution for 45 min and rinsing once in distilled water
5. Staining in Ponceau Fuchsin Solution for 3 min and then rinsing in distilled water
6. The slides were incubated in Phosphotungstic Acid (1%) until the muscles were red and the background pale pink, then rinsing in distilled water
7. Staining with Aniline Blue solution for 1 hour and rinsing several times in distilled water
8. Dehydration of the slides, washing them in Xylene and covering them using a coverslip with glycerol

The results of the Carstairs staining can be interpreted with the help of the following table (Table 10).

**Table 10 Interpretation of colours obtained by Carstairs' staining.**

Source: https://www.emsdiasum.com/microscopy/technical/datasheet/26381.aspx

| **Fixation Time:** | **48 Hours or more** | **Less than 48 hours** |
|---|---|---|
| Fibrin | Bright Red | Orange to Orange Red |
| Platelets | Gray Blue or Navy | Light Gray |
| Collagen | Bright Blue | Bright Blue |
| Muscle | Red | Red |
| Red Blood Cells | Clear Yellow | Red, Green, or Yellow |

## 2.12 Flow-Based Assay (pilot experiment)

To set up the pilot experiment for the flow chamber assay, existing protocols[68] were adapted for the particular needs of the present study. Two Perfusor Pumps Alaris GH which allow adjustment of the flow rate and pressure were used. The pipe system used a standard model of interchangeable flow so that the flow direction was always kept in the same direction (Figure 13). The pipe connections were Luer-type perfusor connections. An Ibidi chamber slide was then connected to the pipe system and to the perfusor syringes. Great care was taken at set-up to remove all air from the system, as bubbles can block the slide or impair image quality under the microscope.

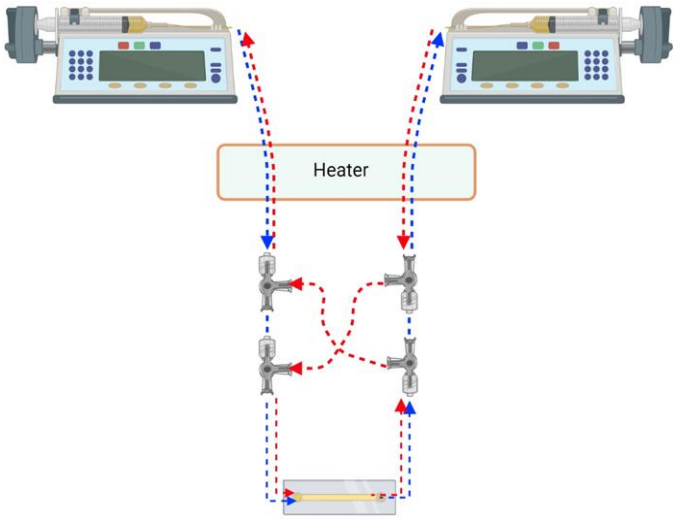


**Figure 13 Flow-Chamber experimental setup**
The diagram shows the completed setup of the flow chamber ready to be observed under a microscope. The direction of the flow is marked, forward flow (blue) and backward flow (red). Due to the intersection in the middle the flow in the slide is unidirectional, as the liquid moves from one pump to the other. A heater was used to maintain a temperature of 37°C in the system.
Created with BioRender.com

We tested several methods of attaching a substance of interest to the slide. Fixation with poly-L-lysine or just letting a layer of the substance to dry inside the channel and used the latter procedure due to better reproducibility.

A few µL of the plaque material were pipetted inside the slide channel and left to incubate at RT for 15-30 min. Afterwards, the rest of the fluid suspension was removed with a pipette. After that, the slide was closed using the Ibidi cover slides and connected to the rest of the system. From this point onward, the chamber slide could be perfused with

different media such as PBS or PPP and the growth of the thrombus as triggered by the plaque could directly be observed in real time under an epifluorescent microscope.

### 2.13 Confocal Laser Microscopy

A Zeiss LSM 510 meta confocal microscope was used for producing IHC images. A confocal laser microscope is based on fluorescence microscopy and has lasers as sources of light, that can excite different dyes. The confocal microscope has a pinhole in the light path, to eliminate scattered light during image acquisition. The laser is equipped with an Argon laser for the following frequencies: 458/477/488/514 nm and has three HeNe lasers for other wavelengths such as 543 nm, 594 nm, and 633 nm. The software used for image acquisition was Zen 2009 by Zeiss. The pictures were taken at the optimal resolution of 1024x1024 pixels with media averaging of 2-4 pictures. The visual field of a single picture at 63x magnification represented a square with sides of 142 µm. The confocal laser microscope was used in this study to observe the IHC stainings (III.2.10).

### 2.14 Epifluorescent scanning microscopy

A Leica SP8X WLL epifluorescence microscope was used to obtain images of the immunohistochemically stained slides. The images were then produced by the microscope's native software, Las X Life Sciences Software Package. Epifluorescent scanning microscopy was used to analyse IHC images, the Flow Chamber experiment, as well as the plaque uptake experiment.

### 2.15 Evaluation of Microscope Images

All images taken on the confocal microscope were analysed using different versions of the ZEN and ZEN lite software packages, provided by Zeiss. The colours and channel intensities in the images were preserved as close as possible to the original settings. Some cell populations were represented as density per visual field (VF). A VF had the following dimensions: 142,7 µm x 142,7 µm. The epifluorescent images were analysed using the native to the microscope software, as well as with ImageJ software.

### 2.16 Statistical analysis

The statistical analysis was carried out using the GraphPad Prism 9 and GraphPad Prism 10 software. Depending on the experimental setup different tests to analyse statistical significance were chosen. For comparing two groups an unpaired Student's t-test was used. When the parameters for Gaussian distribution were not met, a Mann-Whitney test was used. For comparing three sets of data with one variable an ordinary one-way ANOVA test was used, assuming equal standard deviations. For multiple sets of data and

two variables, a two-way ANOVA test was used. Both ANOVA analyses were followed by Fisher's LSD Test for the individual comparisons between the groups. Levels of significance: *p<0.05, **p <0.01, ***p<0.001 and ****p<0.0001.

## IV. Results

### 1. Overall composition of carotid and femoral thrombi

Initially, human thrombi samples were stained exploratively with an HE-staining to determine their composition and to identify relevant components for further experiments. The focus was on the luminal areas, where the plaque had ruptured, and the vessel occlusion took place (Figure 14).

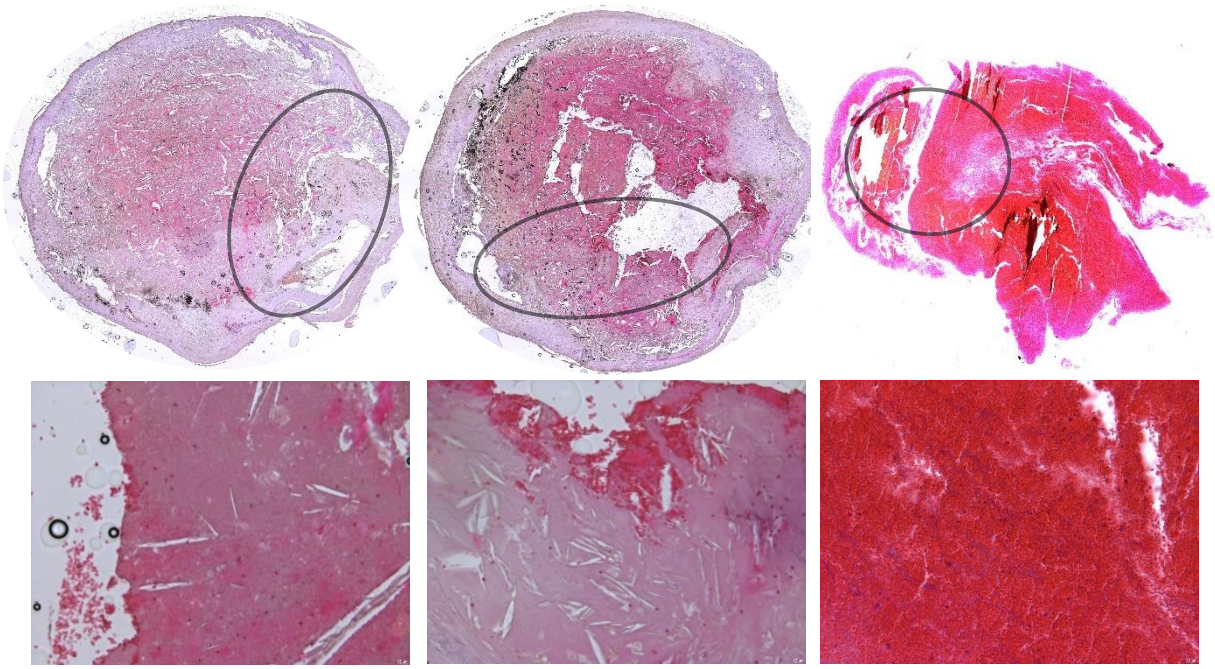

**Figure 14 Representative HE stainings of human arterial thrombi**
Images of femoral thrombi (top). The circled area represents the area towards the vessel lumen, the point of contact with the blood flow and where atherothrombosis took place. On the bottom row - presence of clefts, indicating cholesterol crystals (bottom left and middle), red blood cells and leukocytes (bottom right). Representative images of three different thrombi.

The portions of the thrombi directed towards the vessel lumen, were composed mainly of red blood cells and connective tissue or of platelets, red blood cells and leukocytes (Figure 14). In other parts of the thrombi localised close to the vessel lumen, the typical clefts remaining from cholesterol crystals could be observed (Figure 14). Due to the solvents used when preparing the microscope slides and the staining, the crystals had been dissolved and only their clefts and contours remained. The results suggested that the cholesterol crystals can, in principle, come into contact with blood upon plaque rupture (black circled areas Figure 14), which was further investigated in-vitro (see IV.5.1).

The arterial plaques and thrombi samples were also analysed with a Carstairs staining. This staining method allows for the detection of fibrin, collagen, and platelets, as well as

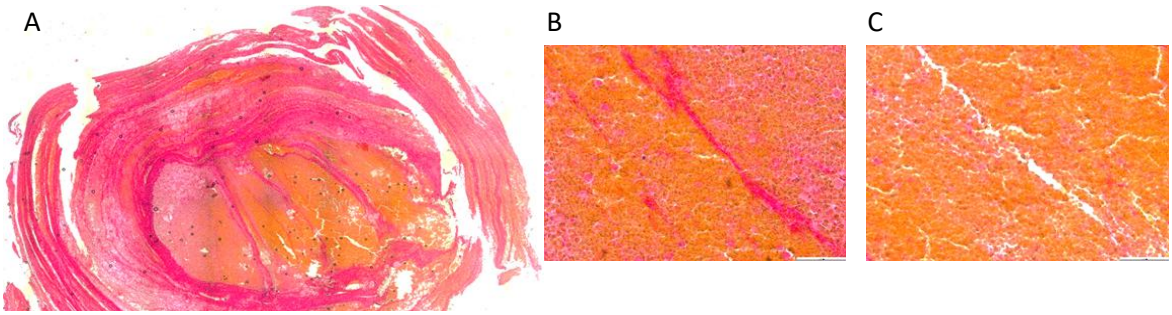


**Figure 15 Carstairs staining of a representative human arterial thrombus (femoral artery)**
A) Overview image.
B) Thrombus section interwoven with fibrin strands.
C) Thrombus section depicting a fibrin and collagen poor area comprised mostly of platelets and erythrocytes.
Representative images of two different thrombi.

observation of their colocalization with red blood cells. An abundance of fibrin was detected and also platelets, which were densely colocalised around the fibrin strands throughout the thrombus (Figure 15).

Next, cellular, and certain molecular components of the thrombi were investigated in more detail.

## 2. Staining of fibrin, platelets, and neutrophils in arterial thrombi

First, we visualised fibrin and platelets as the two core components of plaque-induced thrombi. We observed close colocalizations of nucleated cells (leukocytes) with strands of fibrin and aggregates of red blood cells (Figure 16A). We also visualized the colocalization of thrombocytes and leukocytes (Figure 16B).

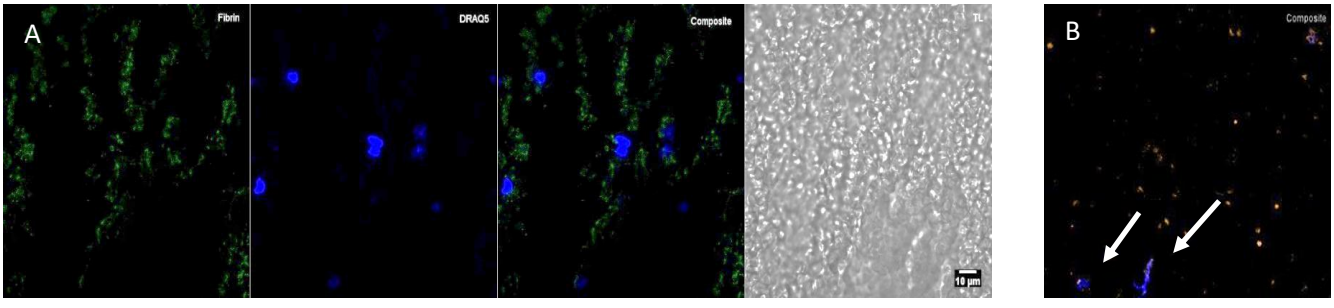


**Figure 16 Presence of fibrin and platelets in human carotid plaque-induced thrombi**
A) A thrombus section depicting fibrin strands (green) and nuclei (blue) of leukocytes. Last image in the series is transmission light (TL). Representative images of two stainings.
B) A thrombus section depicting platelets (yellow) and nuclei (blue) of leukocytes and their colocalization (white arrows).
Representative images of two different thrombi.

NETs and neutrophils were observed to be present in the plaque-induced thrombi (Figure 17) thus opening the possibility of them having an impact on the early thrombus formation upon plaque rupture. Neutrophils were also observed directly interacting with platelets (Figure 18).

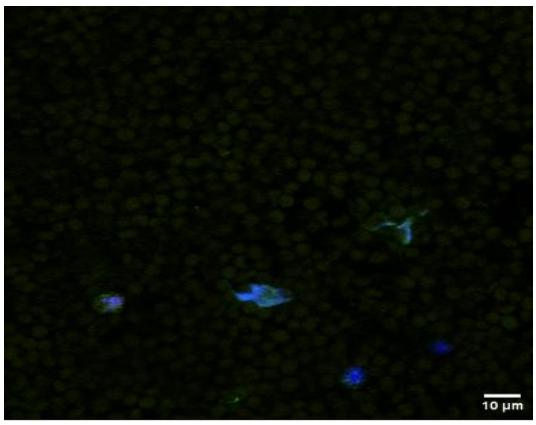


**Figure 17 Presence of neutrophils and NETS femoral thrombus**
MPO (green) and H3cit (orange) with DRAQ5 (blue) for NETs. Purple depicts the overlap of MPO and H3cit. Representative image of two different thrombi.

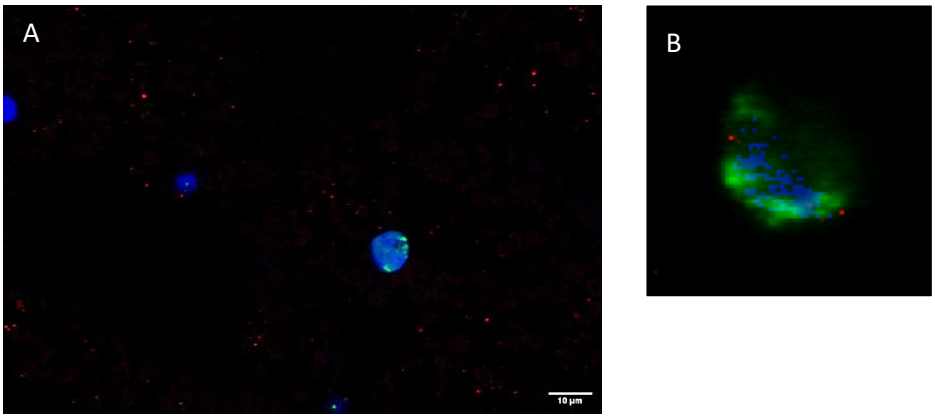


**Figure 18 Colocalization of neutrophils and platelets**
A) Overview of a thrombus IHC staining with platelets (CD41 - red), neutrophils (MPO - green) and nuclei of leukocytes (DAPI - blue).
B) Single neutrophil decorated with platelets.
Representative Images of five different thrombi.

## 3. Pan T-cell and $CD4^+$ T cells IHC staining of human thrombi samples

The localisations and cell to cell interactions of T cells in human arterial thrombi are not completely known. Using the pan T cell marker CD3, we identified 1.73 +/- 0.57 T cells per visual field in arterial atherosclerotic thrombi (Table 11, n=3). One sample (G100.19) was further stained for CD4, where 54% of the T cells were $CD3^+CD4^+$ (n=1, per 10 VF: 6 $CD3^+CD4^+$ T cells). Interestingly several $CD4^+$ T cells interacted with platelets (Figure 19). The T helper cells were mostly of the Th17 subgroup and were shown to cluster among each other or with another subtype of $CD4^+$ T cells (Figure 20, Table 12).

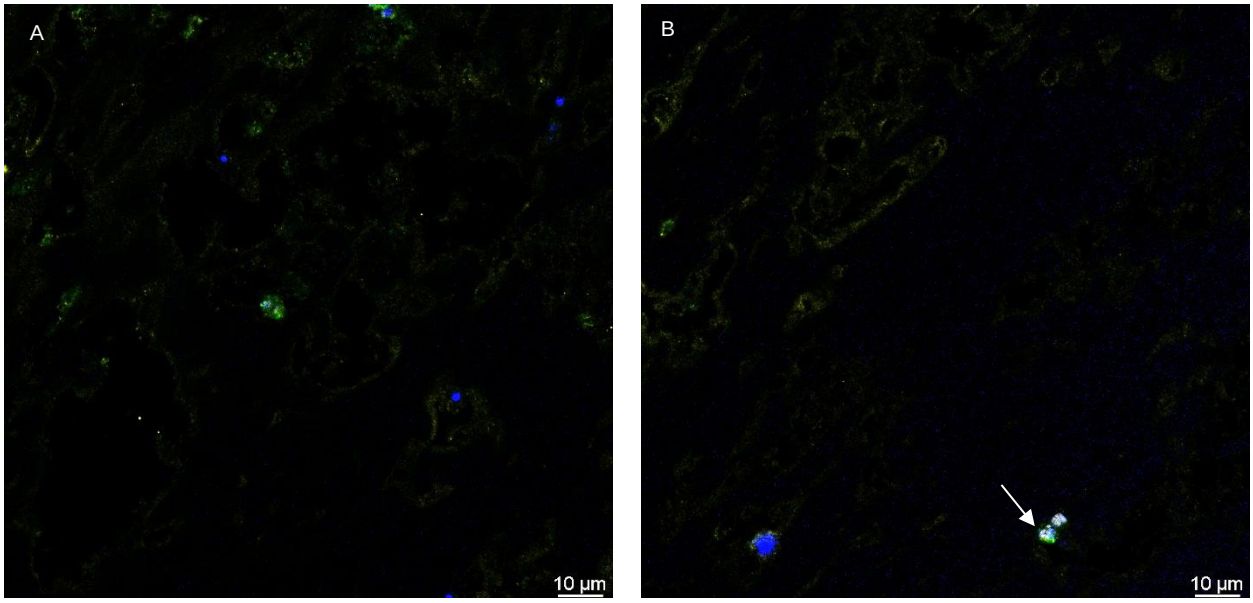


**Figure 19 Colocalization of CD4+ T cells with platelets in femoral thrombi**
Image A and B - Thrombus stainings depicting a colocalization of a CD4+ T cell (CD4 – green, DRAQ5 – red) and platelets (CD41 – yellow).
Representative images of three different thrombi.

**Table 11 T-cell counts in arterial thrombi from 3 patients with PAD**

| Sample | CD3+ DRAQ5+ / 10 VF |
|---|---|
| G138.17 | 18 cells |
| G142.17 | 23 cells |
| G100.19 | 11 cells |

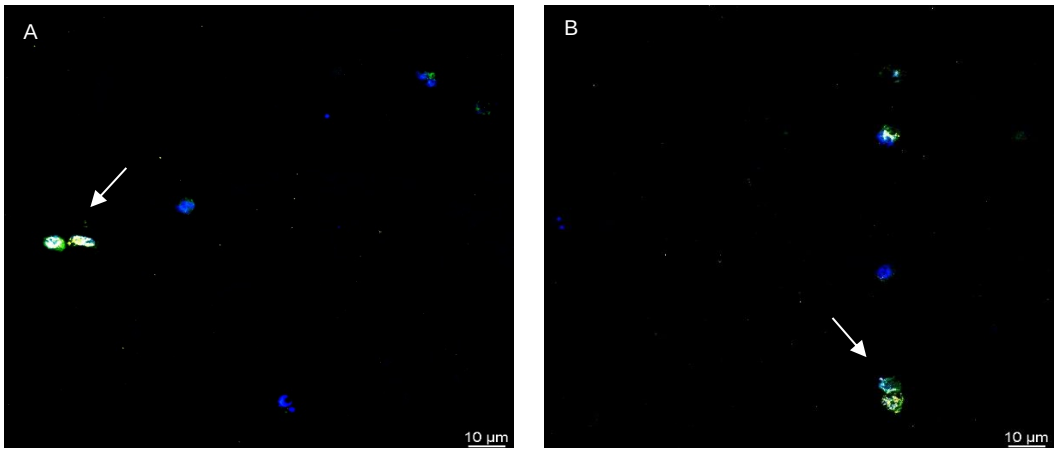


**Figure 20 Presence of Th17 T cells in human arterial Thrombi**

A) Cluster of Th17+ CD4+ T cells (CD4-green, RORγt-yellow, DRAQ5-blue)
B) Cluster of Th17+ CD4+ T cells with another subtype of $CD4^+$ T cell (CD4-green, RORγt-yellow, DRAQ5-blue).
Representative images of three different thrombi.

**Table 12 Distribution of $CD4^+$ and $CD4^+$ $ROR\gamma t^+$ T cells in human carotid samples**

| Sample | CD4+ T cells / 10 VF | CD4+ RORγt + / 10 VF |
|---|---|---|
| G214.19 | 3 cells | 4 cells |
| G138.17 | 2 cells | 2 cells |
| G87.16 | 2 cells | 3 cells |

## 4. In vitro plaque-induced thrombus build up and plaque uptake

A flow chamber with human PPP was set up to examine in real time the interactions and colocalizations between immune cells and other cells with plaque material ex vivo. We observed cell build up on top of the prothrombotic material, and buildup of cell clusters on top of a fibrin clot (Figure 21). An adherence and colocalization between a B-lymphocyte and other cells could also be visualised (Figure 22).

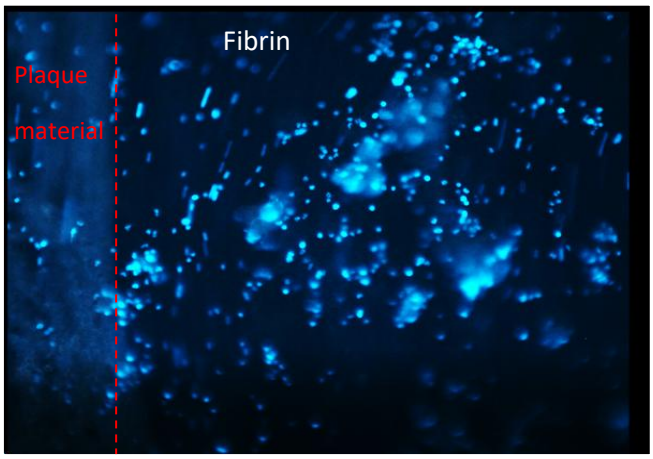


**Figure 21 Flow Chamber – plaque-induced Thrombus in PPP and cell build-up**
Depicted is the fibrin clot build up next to the plaque material (left side). Clusters of PBMCs (DAPI, blue) on top of the fibrin clot are visible. Elongated nuclei represent cells in movement. Image shown is from a single pilot experiment.

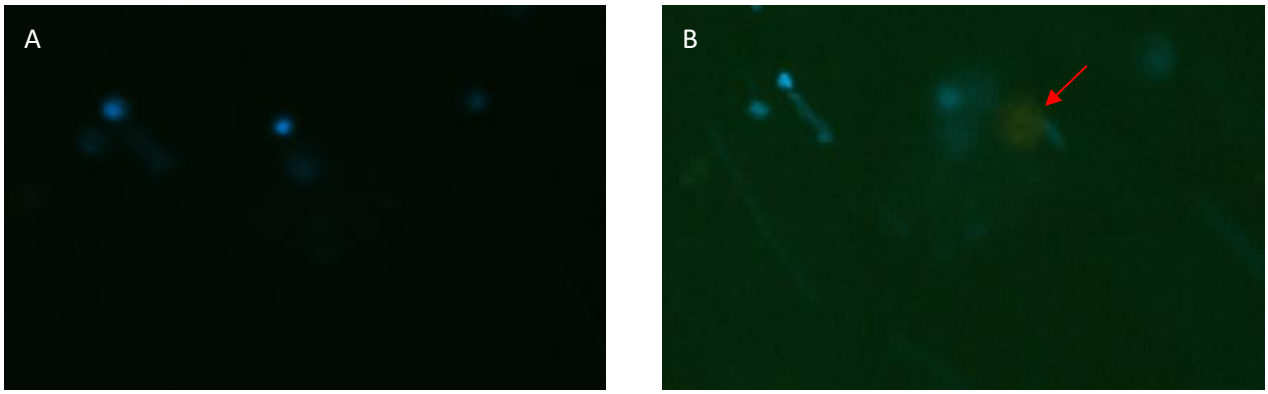


**Figure 22 Flow Chamber – Monocytes/B cells in plaque-induced Thrombus in PPP**
Macrophages/Monocytes (CD14 – blue), B cells (CD19 – orange)
A) Visualisation of stationary $CD14^+$ cells on top of the fibrin clot.
B) $CD19^+$ cells interacting with a cluster of $CD14^+$ cells.
Images shown are from a single pilot experiment.

Next, we visualised the cell-to-cell interaction between the homogenised plaque material and PBMCs. Colocalization was observed of single cells or clustered cells with the labelled plaque material (Figure 23).

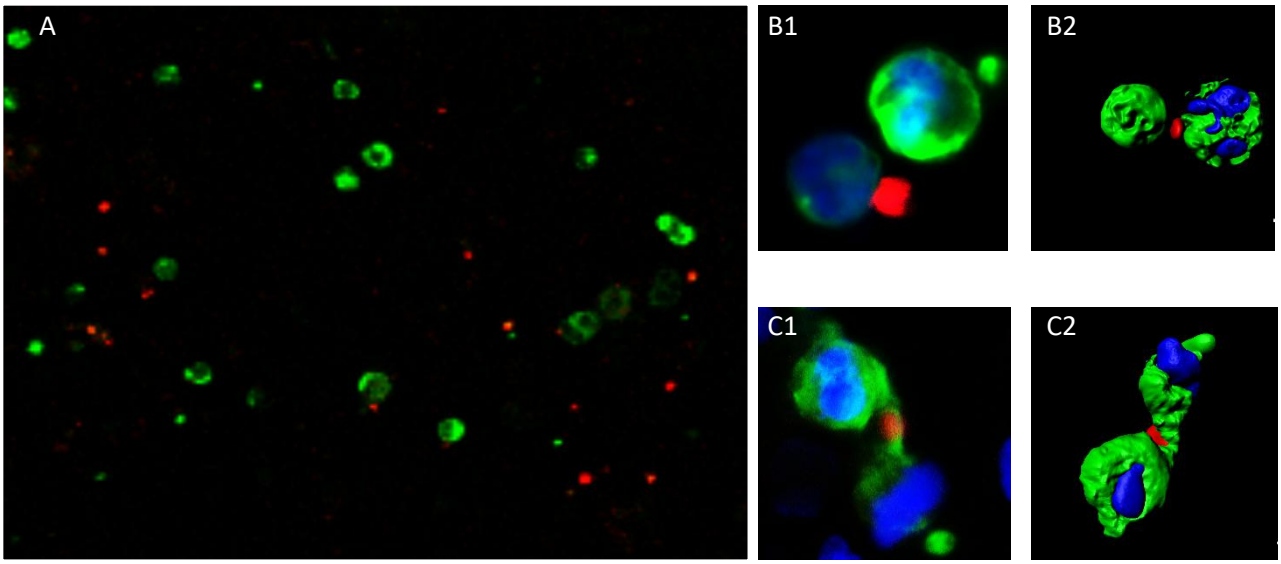


**Figure 23 Interaction between PBMCs and Plaque material 1h and 4h Incubation in-vitro**
Representative images cell to plaque material and cell to cell Interaction
A) Overview image 4h incubation: PBMCs - green, plaque material - red
B1) Cluster of PBMCs interacting with plaque material - 1h incubation B2) 3D image of B1
C1) Cluster of PBMCs interacting with plaque material - 4h incubation C2) 3D image of C1
Images shown are representative of three different thrombi.

## 5. Effects of atherosclerotic plaques on human whole blood coagulation

### 5.1 Effects of cholesterol crystals on human whole blood

Since cholesterol crystals (CCs) were detected in the arterial thrombi (see IV 1.), we further studied the effects of isolated CCs on whole blood coagulation. In the first experimental setup, cholesterol crystals were added in different concentrations to human whole blood (Figure 24).

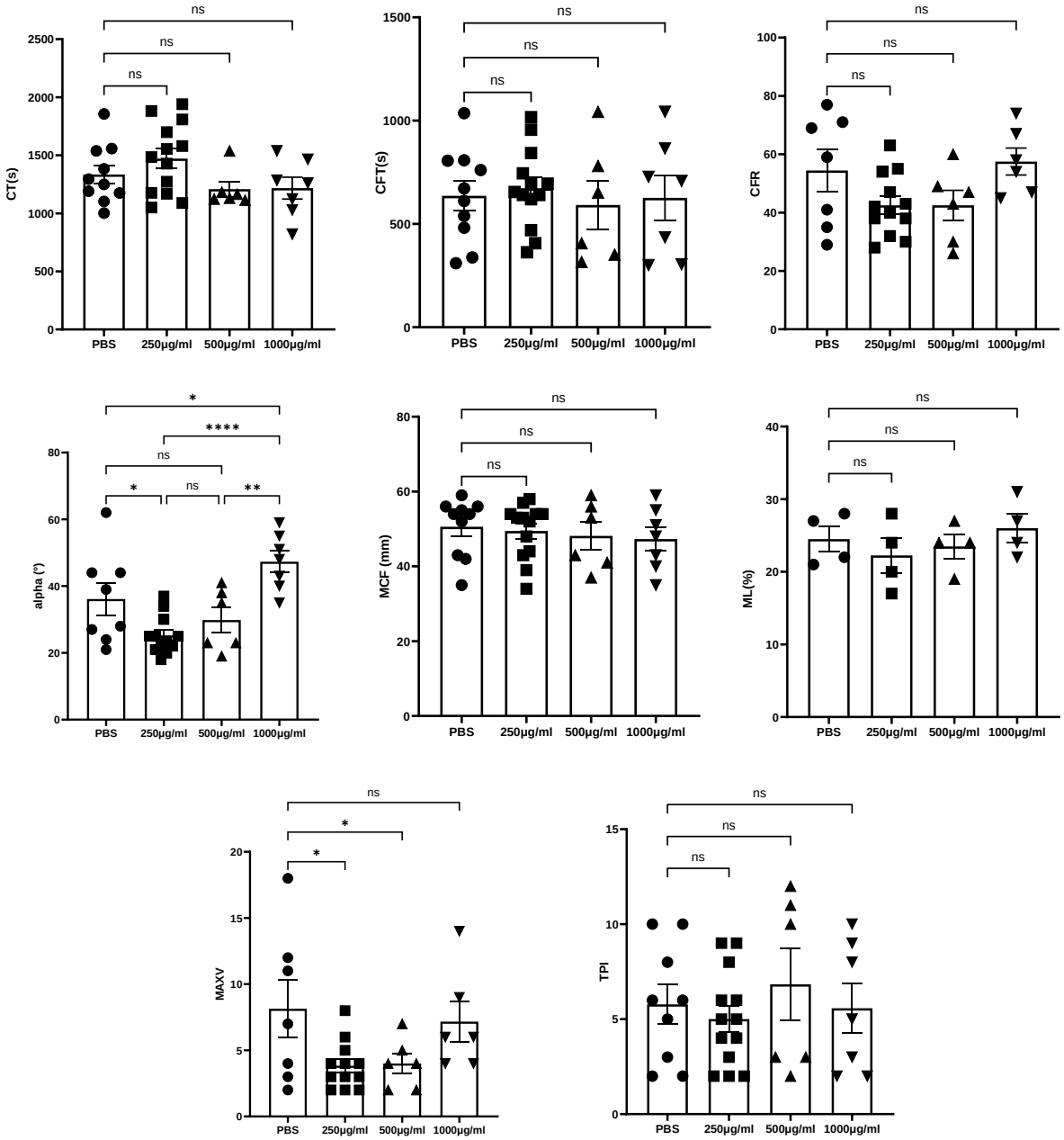


**Figure 24 Effects of cholesterol crystals on human whole blood coagulation**
CT, CFT, CFR, alpha°, MCF, ML, MAXV and TPI parameters for human whole blood supplemented with cholesterol crystals in 3 different concentrations: 250 µg/ml, 500 µg/ml, and 1000 µg/ml. Each of the different symbols represent a different measurement. The data is represented as mean values +/- SEM (n=7, independent biological replicates). Each data point represents a single channel measurement. The p value was calculated using a one-way ANOVA test with the following significance levels: *p<0.05; **p<0.01; ***p<0.001; ****p<0.0001

The following parameters were examined to fully assess the effects of CCs on the whole blood coagulation: coagulation time (CT), clot formation time (CFT), clot formation rate (CFR), maximum clot firmness (MCF), alpha angle (alpha°), maximum lysis (ML), maximum velocity (MAXV) and total prothrombotic index (TPI).

The cholesterol crystals did not show effects on the CT, CFT or CFR. CCs at a concentration of 250 µg/ml and at 1000 µg/ml reduced the alpha°, suggesting that the speed at which the thrombus forms after the onset of coagulation was reduced. However, addition of 1000 µg/ml CCs significantly increased the alpha° compared to the control and the 250 µg/ml group. MCF and ML parameters were unchanged by CCs. At low concentrations of CCs, the MAXV value was reduced indicating that the crystals had reduced the maximal velocity of thrombus formation (Figure 24). Overall, CCs thus decreased thrombus formation in whole blood.

### 5.2 Effects of homogenised plaque material on human whole blood

Next, we studied how atherosclerotic plaques affected whole blood coagulation. Homogenised plaques were added to human whole blood ex vivo (Figure 25). The plaques induced a strong decrease in CT and CFT values (Figure 25) and increased the alpha°, consistent with substantial increases in thrombus formation. The mean TPI value was also significantly increased, indicating a hypercoagulable state.

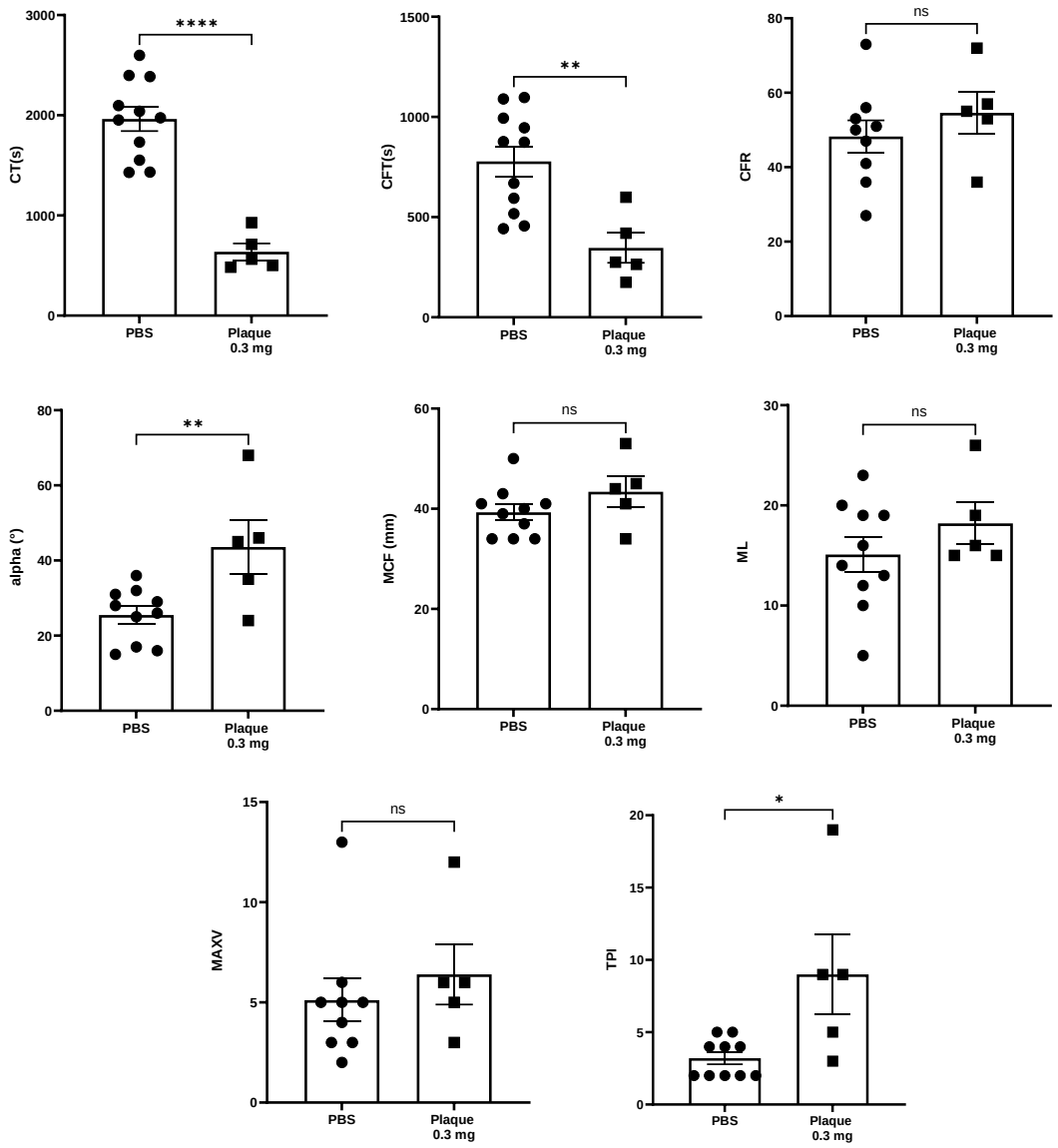


**Figure 25 Effects of homogenised atherosclerotic plaques on whole blood coagulation**
CT, CFT, CFR, alpha°, MCF, ML, MAXV and TPI values for human whole blood supplemented with homogenised carotid atherosclerotic plaques (0.3mg). Each of the different symbols represents a different measurement. The data is represented as mean values +/- SEM (n=6, independent biological replicates). Each data point represents a single channel measurement. The p value was calculated using an unpaired t-test with the following significance levels: *p<0.05; **p<0.01; ***p<0.001; ****p<0.0001

## 5.3 Effects of homogenised plaque material on human platelet poor plasma (PPP)

To analyse whether the activator of the contact pathway of coagulation, factor XII, was involved in thrombus formation upon plaque rupture, we added homogenised plaques to human PPP, compared with FXII deficient human PPP (Figure 26).

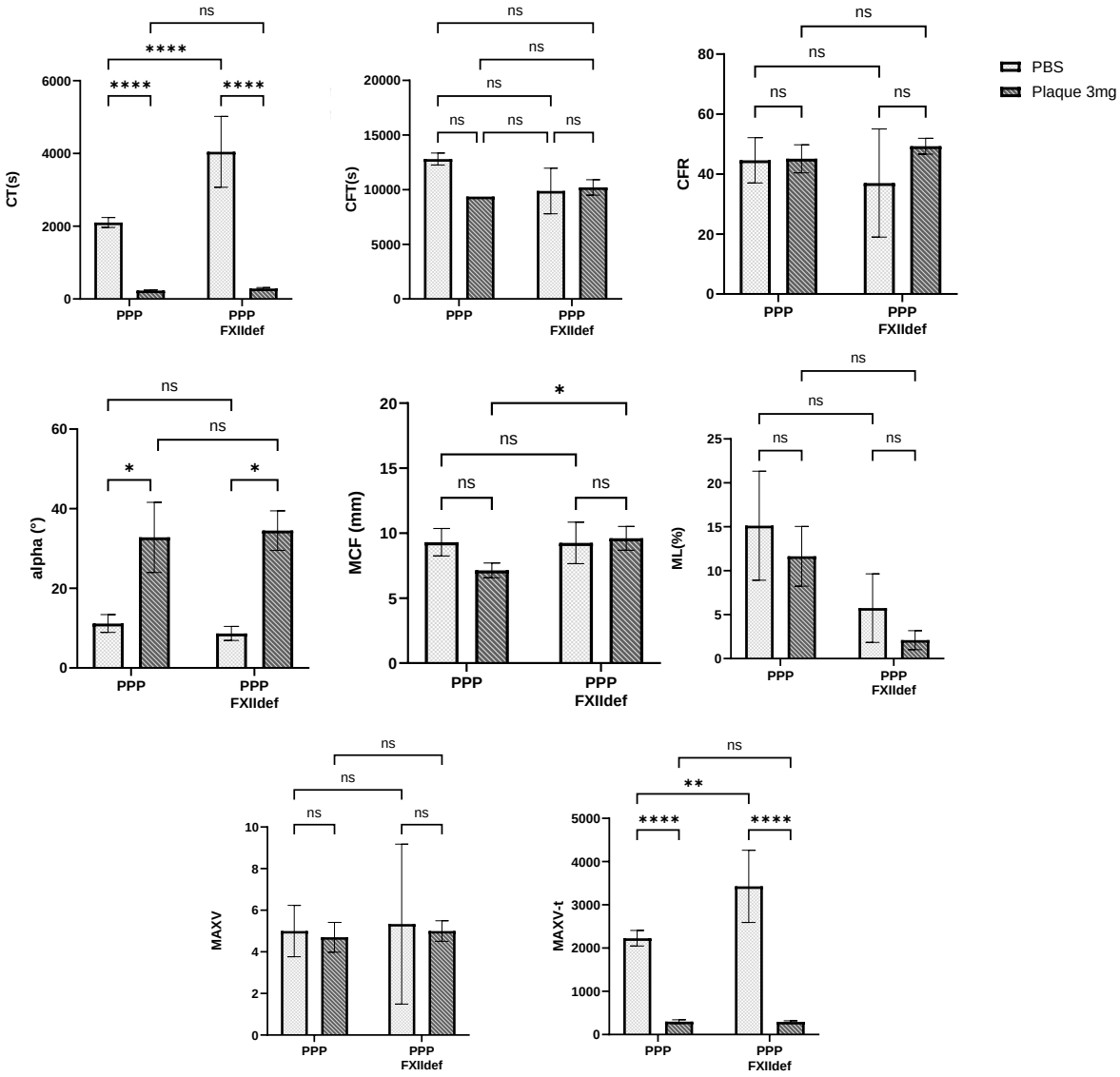


**Figure 26 Effects of atherosclerotic plaque material on human PPP with or without FXII**
CT, CFT, CFR, alpha°, MCF, ML, MAXV and MAXV-t parameters for PPP with or without FXII and supplemented with carotid atherosclerotic plaques (3mg). The data is represented as mean values +/- SEM (n= 3-10, independent biological replicates). Each data point represents a single channel measurement. The p value was calculated using a two-way ANOVA test with the following significance levels: *p<0.05; **p<0.01; ***p<0.001; ****p<0.0001

In the case of human PPP, large amounts of atherosclerotic plaque are necessary (3mg) to evoke a procoagulant response (Figure 26). Due to the lack of cellular components, no TPI value could be measured. In the absence of plaque, FXII deficiency significantly prolonged the CT value (Figure 26). However, the ability of the plaques to enhance

coagulation was not affected by the absence of FXII. The alpha° value was increased in the presence of the atherosclerotic plaques. In the presence of plaques FXII slightly increased the MCF value (Figure 26) in PPP. This suggested a moderate stabilising effect of FXII on plaque-induced clot formation.

MAXV-t was prolonged in FXII deficient PPP in the absence of plaques. Nonetheless, atherosclerotic plaques, significantly reduce MAXV-t (Figure 26) both in normal and in FXII-deficient PPP.

### 5.4 Effects of homogenised plaque material on mouse whole blood

The role of factor XII was further investigated ex vivo using whole blood recovered from WT mice and $FXII^{-/-}$ mice. Atherosclerotic plaques increased plaque-induced fibrin formation both in WT and $FXII^{-/-}$ mice (Figure 27). Moreover, in WT mice plaques increased alpha° more strongly than in $FXII^{-/-}$ mice. MCF was decreased in $FXII^{-/-}$ mice compared to WT mice in the presence of plaques (Figure 27) which contrasts with the results in PPP. The TPI, which represents a parameter that could indicate a propensity towards thromboembolic complication[69] was lower in WT and $FXII^{-/-}$ mice in the presence of plaques.

Thus, blood-based FXII appears to enhance the speed of fibrin formation (alpha°), thrombus stability (MCF) and the propensity for activation of the coagulation system as a whole (TPI) in the presence of plaques. Therefore, while atherosclerotic plaques are already potent inducers of fibrin formation, the presence of blood-based coagulant Factor XII might contribute to enhancing arterial thrombosis after plaque rupture.

Although comparisons between mouse and human blood or PPP and the mixing of human plaque with mouse blood need to be treated with caution, the results in Figure 26 and Figure 27 could suggest, that the stabilising effect of FXII on thrombosis requires the presence of platelets and/or immune cells.

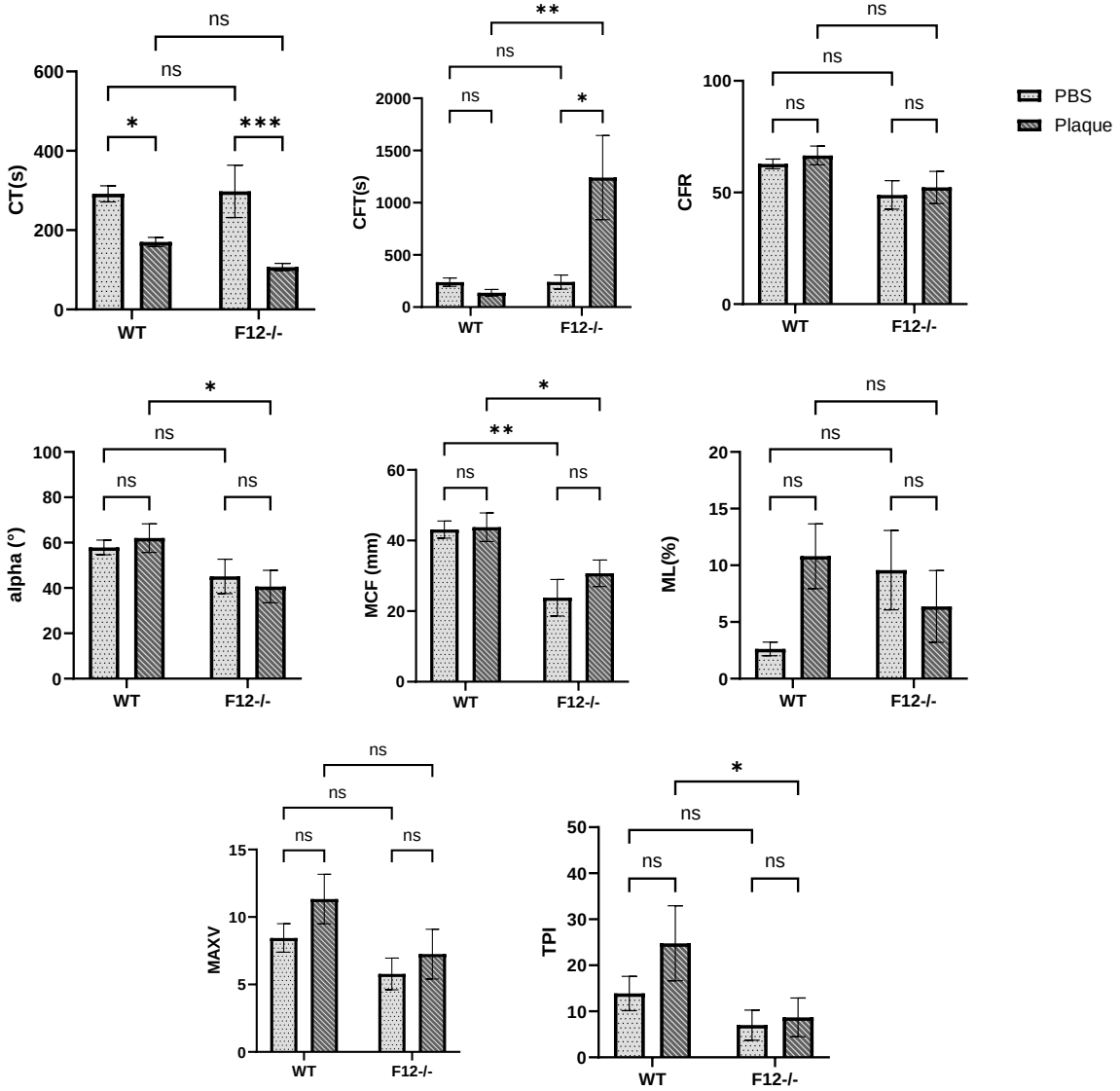


**Figure 27 Effects of plaque material on whole blood from WT and FXII$^{-/-}$ mice**
CT, CFT, alpha°, MCF, ML, MAXV and TPI values for mouse whole blood supplemented with 0.3mg human carotid atherosclerotic plaque. Comparison between WT-WB and F12$^{-/-}$ WB. The data is represented as mean values +/- SEM (n= 4-11, independent biological replicates). Each data point represents a single channel measurement. The p value was calculated using a two-way ANOVA test with the following significance levels: *p<0.05; **p<0.01; ***p<0.001.

## 5.5 Effects of classical monocytes on the coagulation process in the presence of atherosclerotic plaque material

Given the indication that immune cells contribute, along with components of the coagulation system to thrombus stability, we next investigated the role of different immune cells in the plaque-induced thrombus formation. We first examined the role of classical monocytes because they are known to initiate the extrinsic pathway of coagulation when activated. Furthermore, as one of the first cells involved in atheroprogression, they have been also shown to directly interact with $CD4^+$ T cells by presenting antigens to them, further enhancing atheroprogression[70]. Classical monocytes were isolated from human blood, activated with LPS, and then added to the ROTEM device (Figure 28).

Activated, but not resting, classical monocytes reduced the CT and CFT values and increased CFR and alpha° compared to the values measured with plaques alone. Activated classical monocytes also enhanced the stability of the thrombi (MCF) compared to non-activated monocytes. Resting classical monocytes instead increased the lysis of plaque-induced thrombi, compared to plaque-induced thrombus formation, potentially due to a fibrinolytic activity of the cells (ML). Activated classical monocytes increased the maximum velocity of thrombus formation and the time to reach it (MAXV-t and MAXV parameters), thus overall increasing the TPI value (Figure 28).

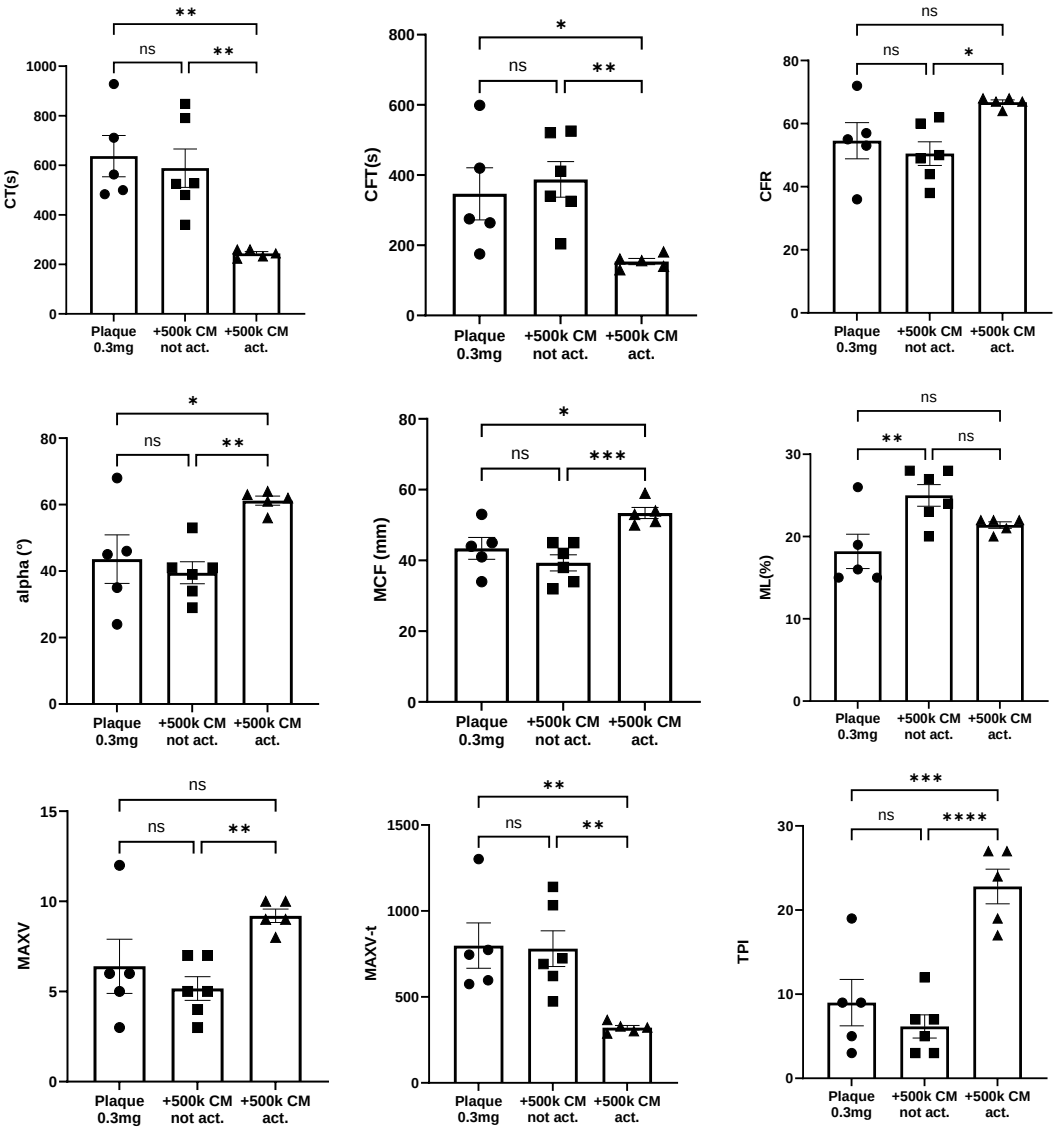


**Figure 28 Effects of classical monocytes on coagulation**

CT, CFT, CFR, alpha°, MCF, ML, MAXV, MAXV-t and TPI parameters for human whole blood supplemented with 0.3mg atherosclerotic plaque and added $5x10^5$ classical monocytes (not activated/activated). Each of the different symbols represents a different measurement. The data shown for the group with plaque only is the same data as shown in IV.4.5. The data is represented as mean values +/- SEM (n=4, independent biological replicates). Each data point represents a single channel measurement. The p value was calculated using a one-way ANOVA test with the following significance levels: *p<0.05; **p<0.01; ***p<0.001.

Table 13 summarizes the effects of non-activated and activated classical monocytes on the TEG parameters. In additional experiments, non-activated and activated non classical monocytes ($5x10^5$) were assessed under the same conditions as in Figure 28. Non-classical monocytes did not influence the TEG parameters (Table 13).

**Table 13 Comparison of cM and ncM effects on plaque-induced coagulation**
↔ - no significant change, ↑↑ - significant increase, ↑↑ - significant decrease

| Plaque + | cM non-activ. | cM activ. | ncM non-activ. | ncM activ. |
|---|---|---|---|---|
| CT | ↔ | ↓↓ | ↔ | ↔ |
| CFT | ↔ | ↓↓ | ↔ | ↔ |
| CFR | ↔ | ↑↑ | ↔ | ↔ |
| alpha | ↔ | ↑↑ | ↔ | ↔ |
| MCF | ↔ | ↑↑ | ↔ | ↔ |
| ML | ↑↑ | ↔ | ↔ | ↔ |
| MAXV | ↔ | ↑↑ | ↔ | ↔ |
| MAXV-t | ↔ | ↓↓ | ↔ | ↔ |
| TPI | ↔ | ↑↑ | ↔ | ↔ |

## 5.6 Effect of $CD4^+$ T cells on plaque-induced thrombus formation

Next, we studied the role of $CD4^+$ T cells in plaque-induced thrombus formation. This cell type was chosen because parallel experiments in our laboratory suggested that $CD4^+$ T cells could regulate microvascular thrombosis in infection. Given the range of 500-1500 $CD4^+$ T cells/μL in healthy adults, the cell counts chosen mimicked these physiological values. Resting $CD4^+$ T cells at a concentration of $5x10^5$ per TEG channel significantly increased CFT values, thus demonstrating a delay in thrombus formation. No other significant differences in the parameters were observed (Figure 29).

To assess whether the effect of the $CD4^+$ T cells was dependent on T cell activation, the T cells were activated with CD3/CD28 complex to mimic their activation via TCR stimulation. Activated $CD4^+$ T cells at a concentration of $5x10^5$ tended to increase the CFT parameter but otherwise did not change any of the other thrombus parameters (Figure 29).

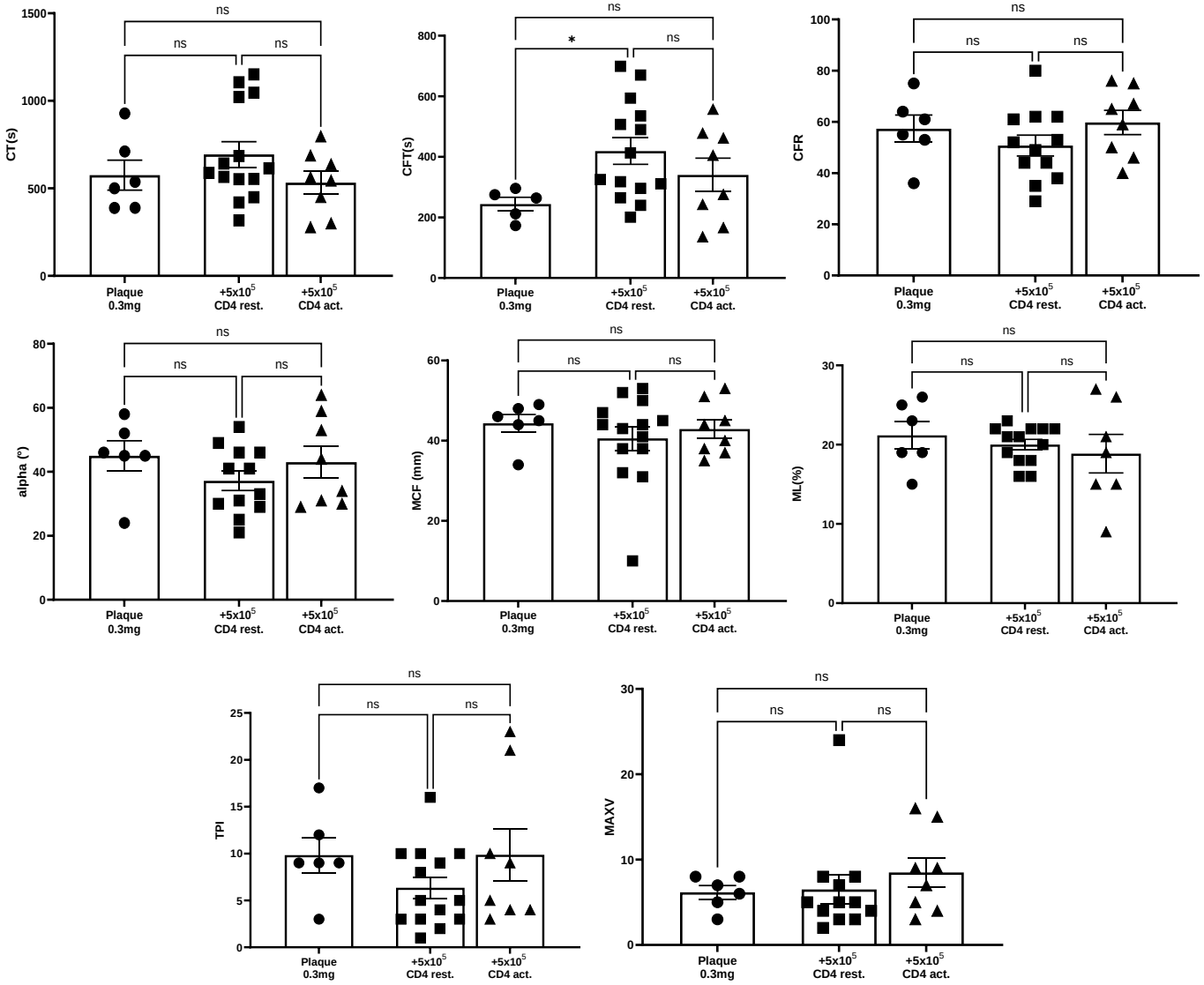


**Figure 29 Effects of activated/resting CD4⁺ T cells on plaque-induced thrombus formation.**
CT, CFT, CFR, Alpha angle, MCF, ML, TPI and MAXV parameters for whole blood supplemented with atherosclerotic plaque material (0,3mg) and CD4⁺ T cells ($5x10^5$ resting/activated cells). Each of the different symbols represents a different measurement. The data is represented as mean values +/- SEM (n=4-7, independent biological replicates). Each data point represents a single channel measurement. The p value was calculated using a one-way ANOVA test with the following significance levels: *p<0.05.

## 5.7 Involvement of PAI-1 in plaque-induced thrombus formation.

PAI-1 is thought to be a major trigger of arterial thrombosis. We used anti-PAI-1 antibody to neutralise PAI-1 during plaque-driven thrombus formation. Anti-PAI-1 tended to decrease fibrin formation (CT) and reduce the alpha angle (Figure 30). Notably, PAI-1 inhibition prolonged the time interval to reach the maximal velocity of thrombus formation (MAXV-t). This suggested that PAI-1 contributes to human arterial thrombosis induced by atherosclerotic plaques.

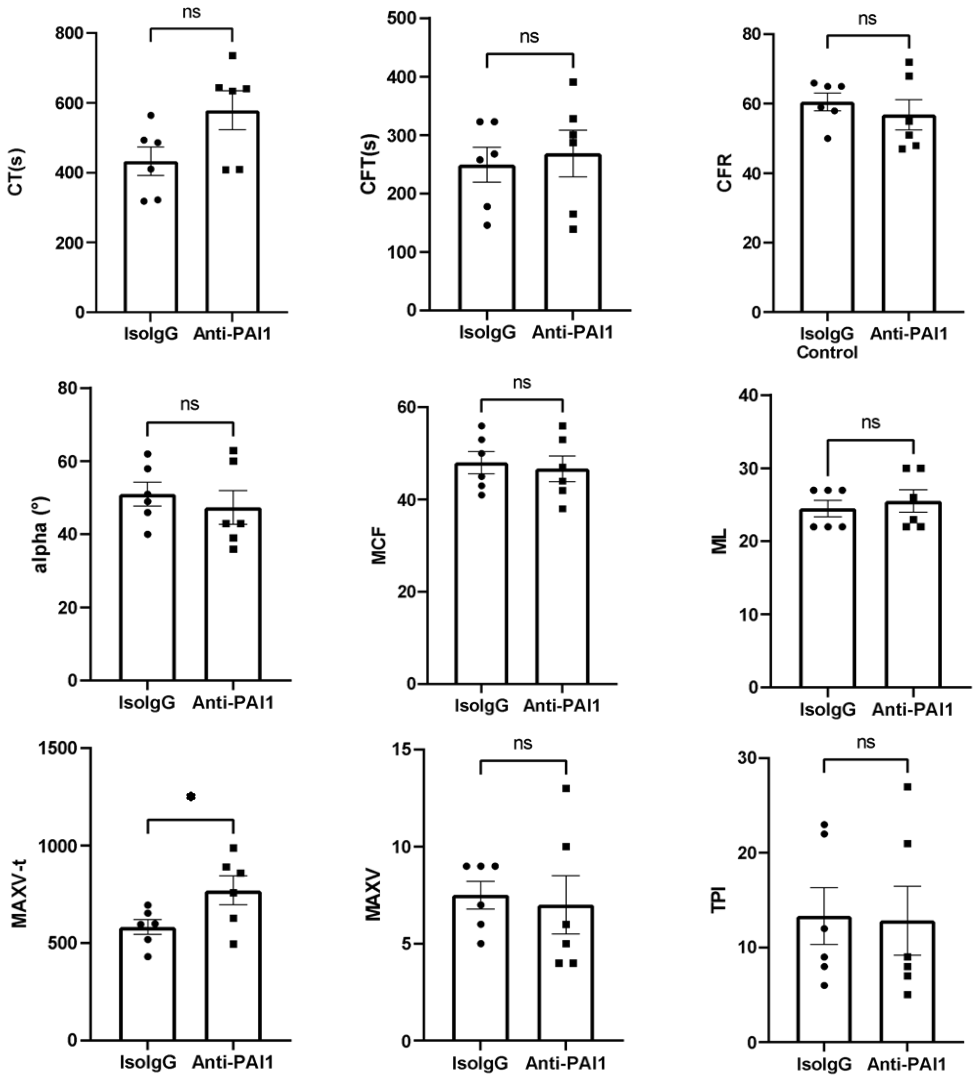


**Figure 30 Effects of neutralising PAI-1 on plaque-induced thrombus development**
CT, CFT, CFR, alpha angle, MCF, ML, MAXV and TPI parameters for whole blood supplemented with atherosclerotic plaque material (0.3mg) and Anti-PAI1 (2,4 µg). Each of the different symbols represents a different measurement. The data is represented as mean values +/- SEM (n=3, independent biological replicates). Each data point represents a single channel measurement. The p value was calculated using an unpaired t-test with the following significance levels: *p<0.05.

## V. Discussion

Atherosclerosis is one of the most common vascular pathologies contributing strongly to overall cardiovascular disease and mortality. Atherosclerosis becomes a life-threatening disease when it develops into atherothrombosis. Arterial thrombosis is thus a leading cause of global morbidity and mortality. Our goal was to gain further insight into the immune cells involved in acute carotid and femoral arterial thrombosis induced by the rupture of atherosclerotic plaques. Preliminary stainings of arterial thrombi showed that thrombi derived from carotid and femoral arteries were composed mostly of erythrocytes, platelets, fibrin and dispersed leukocytes[71].

Initially we aimed to gather more insight into to the extent to which cholesterol crystals and homogenised plaque material influence coagulation in human blood. These tests were conducted on human whole blood using a ROTEM device, which mimics slow venous flow. The ROTEM device allowed us to observe in real time the effects of atherosclerotic plaque material on the thrombus formation. Cholesterol crystals inside plaques have been shown to have a strong pro-inflammatory role[44]. We assessed their effects on whole blood thrombus formation using 3 different concentrations. None had any effect on the various parameters analysed. Our findings shows that it is unlikely that cholesterol crystals are involved in the early stages of atherothrombosis. On the other hand, cholesterol crystals have been suggested to induce coagulation by complement activation which consequently increases the TF expression of monocytes[72,73]. Thus, cholesterol crystals may be more important for arterial thrombosis development at later stages.

Next, we analysed the effects of atherosclerotic plaques on whole blood fibrin and thrombus formation. We used plaque material from human carotid and femoral arteries dissected under sterile conditions, separating the atheromatous material from the rest of the sample[67]. Upon addition of the plaque material to the blood sample we observed significant decreases in the coagulation time ($p<0.0001$) as well as in the clot formation time ($p=0.0036$) compared to the control values. This is in accordance with earlier works[68,76]. These findings together with an increased TPI index, a measurement of the clumping of red blood cells, confirmed a strong procoagulant effect of the plaque material and its major role in thrombus formation upon plaque rupture[74].

To identify the involvement of blood components in plaque-induced thrombosis, we measured thrombus formation on the ROTEM device using PPP and FXII deficient PPP. We observed that, even without the blood cells, atherosclerotic plaque-initiated thrombus formation, both in the presence and absence of factor XII. There was no significant

difference between the CT values of PPP and FXII deficient PPP. This implies that blood based FXII does not play a major role in the coagulation initiated by plaque material[50,75]. The role of blood based FXII was further explored in whole mouse blood with and without FXII. The lack of FXII in whole mouse blood did not alter the fibrin formation but increased the CFT value. This suggests that FXII is more important for thrombus buildup at later stages as opposed to the initial thrombus buildup[76].

The leukocytes observed in the atherosclerotic plaques were mostly neutrophils and their NETs, as well as $CD4^+$ T cells and their subtype Th17. Both neutrophils and T cells interacted with platelets and proteins implicated in the regulation of fibrinolysis, such as PAI-1.

It is widely known that $CD4^+$ T cells represent the majority of the immune cells in atherosclerotic plaques[77]. Some studies suggest that $CD3^+$ T cells are more strongly present in thrombi which are formed after plaque rupture as compared to during an embolism, vessel stenosis, thrombophilia or endovascular complication after a procedure[78]. We also observed PAI-1 on the cell surface of $CD4^+$ T cells. It is unclear whether activated T helper cells express PAI-1 themselves. Alternatively, PAI-1 present on the surface of T cells could be secreted by platelets or endothelial cells upon plaque rupture. Whether by binding to PAI-1, these cells can act as procoagulant or anticoagulant agents, remains the question of further research. Due to the scope of our stainings, we cannot surely ascertain which exact subtype of the $CD4^+$ T cells , observed in the thrombi, interacted with PAI-1, as once activated the T helper cells can acquire many features aimed at completing different tasks[79]. We further studied this colocalization and its significance in our in-vitro experiments, by replicating a fibrin clot (atherosclerotic plaque activated coagulation mostly through the GPVI platelet receptor) as well as by observing cell adhesion onto the clot, following protocols used in other studies involving flow chambers[80,81].

Next, we aimed to identify to what extent monocytes, the major carriers of intravascular TF, and $CD4^+$ T cells regulate plaque-induced thrombus formation. Preliminary work from our group suggests that intravascular immune cells could affect thrombus formation induced by atherosclerotic plaques. To detail the relevance of blood immune cells in arterial thrombosis we first focused on classical and non-classical monocytes. Although plaques themselves strongly stimulate fibrin formation and thrombus development, this was further enhanced by activated classical monocytes as indicated by the shorter CT and CFT values, as well as increased CFR and MCF values[82].

In contrast, resting classical monocytes, which do not express TF, did not enhance fibrin formation or thrombus development triggered by arterial plaques. Instead, they increased the maximum lysis of the clot, consistent with enhancement of fibrinolysis. Moreover, non-classical monocytes did not influence plaque-induced thrombus formation at all. Thus, our results show that activated classical monocytes amplify plaque-induced thrombosis, whereas non-classical monocytes appear to lose their procoagulant character. This is in line with other works reporting on monocyte conversion in the human model and the role of non-classical monocytes in regulating immune response in CVDs[83].

Single-cell RNA sequencing on atherosclerotic plaques performed in the laboratory of Prof. L. Mägdefessel (TUM) indicated that plaque associated $CD4^+$ T cells expressed elevated levels of negative regulators of coagulation, in particular of fibrinolysis mediators such as uPA and uPAR (data not shown). This is principally in agreement with the presence of PAI-1 on the cell surface of $CD4^+$ T cells since PAI-1 forms a complex with uPA and its receptor uPAR (see above).

However, isolated resting human $CD4^+$ T cells did not affect the coagulation / thrombus parameters in whole blood treated with atherosclerotic plaques. $CD4^+$ T cells activated via TCR-dependent mechanisms were also without effect on the TEG parameters. Potentially the capacity of $CD4^+$ T cells may not be sufficient to counter the strong effects of the plaques.

PAI-1 acts as the main inhibitor of tissue plasminogen activator (tPA) and urokinase (uPA), thus hindering fibrinolysis and promoting thrombus build up[84-86]. Although there are limited studies on the direct effects of PAI-1 upon thrombotic events in humans, there is an abundance of data which describes its presence in the plaques and its causal role in atherosclerotic diseases such as MI[87] and stroke[88], as well as in DVT and microvascular thrombosis.

We also investigated which aspect of plaque-induced thrombus formation can be directly influenced by the presence or lack of PAI-1. To examine the function of plaque-associated PAI-1 we used a neutralising anti PAI-1 antibody. Blocking PAI-1 tended to prolong the CT value, which is consistent with decreased fibrin formation. This is in line with earlier works showing that the lack of PAI-1 leads to higher fibrinolytic activity and slower thrombus buildup[89].

## VI. References


1. WHO. Cardiovascular diseases (CVDs) Fact sheet. https://www.who.int/news-room/fact-sheets/detail/cardiovascular-diseases-(cvds)

2. Global Burden of Disease Study. https://www.healthdata.org/gbd/2019

3. Vos T, Allen C, Arora M, et al. Global, regional, and national incidence, prevalence, and years lived with disability for 310 diseases and injuries, 1990–2015: a systematic analysis for the Global Burden of Disease Study 2015. The Lancet. 2016;388(10053):1545-1602. doi:10.1016/s0140-6736(16)31678-6

4. Fernández-Friera L, Peñalvo JL, Fernández-Ortiz A, et al. Prevalence, Vascular Distribution, and Multiterritorial Extent of Subclinical Atherosclerosis in a Middle-Aged Cohort. Circulation. 2015;131(24):2104-2113. doi:10.1161/circulationaha.114.014310

5. Hopstock LA, Bønaa KH, Eggen AE, et al. Longitudinal and secular trends in total cholesterol levels and impact of lipid-lowering drug use among Norwegian women and men born in 1905–1977 in the population-based Tromsø Study 1979–2016. BMJ Open. 2017;7(8):e015001. doi:10.1136/bmjopen-2016-015001

6. Schreiner PJ, Jacobs DR, Wong ND, Kiefe CI. Twenty-Five Year Secular Trends in Lipids and Modifiable Risk Factors in a Population-Based Biracial Cohort: The Coronary Artery Risk Development in Young Adults (CARDIA) Study, 1985–2011. Journal of the American Heart Association. 2016;5(7)doi:10.1161/jaha.116.003384

7. Ference BA, Ginsberg HN, Graham I, et al. Low-density lipoproteins cause atherosclerotic cardiovascular disease. 1. Evidence from genetic, epidemiologic, and clinical studies. A consensus statement from the European Atherosclerosis Society Consensus Panel. European Heart Journal. 2017;38(32):2459-2472. doi:10.1093/eurheartj/ehx144

8. Nordestgaard BG, Chapman MJ, Humphries SE, et al. Familial hypercholesterolaemia is underdiagnosed and undertreated in the general population: guidance for clinicians to prevent coronary heart disease: Consensus Statement of the European Atherosclerosis Society. European Heart Journal. 2013;34(45):3478-3490. doi:10.1093/eurheartj/eht273

9. Musunuru K, Kathiresan S. Surprises From Genetic Analyses of Lipid Risk Factors for Atherosclerosis. Circulation Research. 2016;118(4):579-585. doi:10.1161/circresaha.115.306398

10. Libby P. Triglycerides on the rise: should we swap seats on the seesaw? European Heart Journal. 2015;36(13):774-776. doi:10.1093/eurheartj/ehu500

11. Rocha VZ, Libby P. Obesity, inflammation, and atherosclerosis. Nature Reviews Cardiology. 2009;6(6):399-409. doi:10.1038/nrcardio.2009.55

12. Cybulsky MI, Gimbrone MA, Jr. Endothelial expression of a mononuclear leukocyte adhesion molecule during atherogenesis. Science. Feb 15 1991;251(4995):788-91. doi:10.1126/science.1990440

13. Li H, Cybulsky MI, Gimbrone MA, Libby P. An atherogenic diet rapidly induces VCAM-1, a cytokine-regulatable mononuclear leukocyte adhesion molecule, in rabbit aortic endothelium. Arteriosclerosis and Thrombosis: A Journal of Vascular Biology. 1993;13(2):197-204. doi:10.1161/01.atv.13.2.197

14. Ignarro LJ, Napoli C. Novel features of nitric oxide, endothelial nitric oxide synthase, and atherosclerosis. Current Diabetes Reports. 2005;5(1):17-23. doi:10.1007/s11892-005-0062-8

15. Chatzizisis YS, Coskun AU, Jonas M, Edelman ER, Feldman CL, Stone PH. Role of endothelial shear stress in the natural history of coronary atherosclerosis and vascular remodeling: molecular, cellular, and vascular behavior. J Am Coll Cardiol. Jun 26 2007;49(25):2379-93. doi:10.1016/j.jacc.2007.02.059

16. Badimon L, Vilahur G. Thrombosis formation on atherosclerotic lesions and plaque rupture. Journal of Internal Medicine. 2014;276(6):618-632. doi:10.1111/joim.12296

17. Gimbrone MA, García-Cardeña G. Endothelial Cell Dysfunction and the Pathobiology of Atherosclerosis. Circulation Research. 2016;118(4):620-636. doi:10.1161/circresaha.115.306301

18. Kapellos TS, Bonaguro L, Gemund I, et al. Human Monocyte Subsets and Phenotypes in Major Chronic Inflammatory Diseases. Front Immunol. 2019;10:2035. doi:10.3389/fimmu.2019.02035

19. Hansson GRK, Libby P, SchöNbeck U, Yan Z-Q. Innate and Adaptive Immunity in the Pathogenesis of Atherosclerosis. Circulation Research. 2002;91(4):281-291. doi:10.1161/01.res.0000029784.15893.10

20. McLeod O, Silveira A, Fredrikson GN, et al. Plasma autoantibodies against apolipoprotein B-100 peptide 210 in subclinical atherosclerosis. Atherosclerosis. 2014;232(1):242-248. doi:10.1016/j.atherosclerosis.2013.11.041

21. Badimon L. Interleukin-18: a potent pro-inflammatory cytokine in atherosclerosis: EXPERT'S PERSPECTIVE. Cardiovascular Research. 2012;96(2):172-175. doi:10.1093/cvr/cvs226

22. Storey R, Vilahur G, Badimon L. Update on lipids, inflammation and atherothrombosis. Thrombosis and Haemostasis. 2011;105(S 06):S34-S42. doi:10.1160/ths10-11-0717

23. Kim K, Shim D, Lee JS, et al. Transcriptome Analysis Reveals Nonfoamy Rather Than Foamy Plaque Macrophages Are Proinflammatory in Atherosclerotic Murine Models. Circulation Research. 2018;123(10):1127-1142. doi:10.1161/circresaha.118.312804

24. Nathanael, Lana, Jeffrey, et al. Regulated Accumulation of Desmosterol Integrates Macrophage Lipid Metabolism and Inflammatory Responses. Cell. 2012;151(1):138-152. doi:10.1016/j.cell.2012.06.054

25. Libby P, Buring JE, Badimon L, et al. Atherosclerosis. Nat Rev Dis Primers. Aug 16 2019;5(1):56. doi:10.1038/s41572-019-0106-z

26. Nus M, Mallat Z. Immune-mediated mechanisms of atherosclerosis and implications for the clinic. Expert Review of Clinical Immunology. 2016;12(11):1217-1237. doi:10.1080/1744666x.2016.1195686

27. Libby P, Hansson GK. Inflammation and Immunity in Diseases of the Arterial Tree. Circulation Research. 2015;116(2):307-311. doi:10.1161/circresaha.116.301313

28. Gräbner R, Lötzer K, Döpping S, et al. Lymphotoxin β receptor signaling promotes tertiary lymphoid organogenesis in the aorta adventitia of aged ApoE−/− mice. Journal of Experimental Medicine. 2009;206(1):233-248. doi:10.1084/jem.20080752

29. Bennett MR, Sinha S, Owens GK. Vascular Smooth Muscle Cells in Atherosclerosis. Circulation Research. 2016;118(4):692-702. doi:10.1161/circresaha.115.306361

30. Kathryn, Tabas I. Macrophages in the Pathogenesis of Atherosclerosis. Cell. 2011;145(3):341-355. doi:10.1016/j.cell.2011.04.005

31. Clarke MCH, Talib S, Figg NL, Bennett MR. Vascular Smooth Muscle Cell Apoptosis Induces Interleukin-1–Directed Inflammation. Circulation Research. 2010;106(2):363-372. doi:10.1161/circresaha.109.208389

32. Wilcox JN, Smith KM, Schwartz SM, Gordon D. Localization of tissue factor in the normal vessel wall and in the atherosclerotic plaque. Proceedings of the National Academy of Sciences. 1989;86(8):2839-2843. doi:10.1073/pnas.86.8.2839

33. Kaikita K, Ogawa H, Yasue H, et al. Tissue Factor Expression on Macrophages in Coronary Plaques in Patients with Unstable Angina. Arteriosclerosis, Thrombosis, and Vascular Biology. 1997;17(10):2232-2237. doi:10.1161/01.atv.17.10.2232

34. Landers SC, Gupta M, Lewis JC. Ultrastructural localization of tissue factor on monocyte-derived macrophages and macrophage foam cells associated with atherosclerotic lesions. Virchows Arch. 1994;425(1):49-54. doi:10.1007/BF00193948

35. Ruiz JL, Hutcheson JD, Aikawa E. Cardiovascular calcification: current controversies and novel concepts. Cardiovasc Pathol. Jul-Aug 2015;24(4):207-12. doi:10.1016/j.carpath.2015.03.002

36. Ruiz JL, Weinbaum S, Aikawa E, Hutcheson JD. Zooming in on the genesis of atherosclerotic plaque microcalcifications. The Journal of Physiology. 2016;594(11):2915-2927. doi:10.1113/jp271339

37. Huang H, Virmani R, Younis H, Burke AP, Kamm RD, Lee RT. The Impact of Calcification on the Biomechanical Stability of Atherosclerotic Plaques. Circulation. 2001;103(8):1051-1056. doi:10.1161/01.cir.103.8.1051

38. Bentzon JF, Otsuka F, Virmani R, Falk E. Mechanisms of Plaque Formation and Rupture. Circulation Research. 2014;114(12):1852-1866. doi:10.1161/circresaha.114.302721

39. Otsuka F, Yasuda S, Noguchi T, Ishibashi-Ueda H. Pathology of coronary atherosclerosis and thrombosis. Cardiovascular Diagnosis and Therapy. 2016;6(4):396-408. doi:10.21037/cdt.2016.06.01

40. Yuan C, Mitsumori LM, Ferguson MS, et al. In Vivo Accuracy of Multispectral Magnetic Resonance Imaging for Identifying Lipid-Rich Necrotic Cores and Intraplaque Hemorrhage in Advanced Human Carotid Plaques. Circulation. 2001;104(17):2051-2056. doi:10.1161/hc4201.097839

41. Giannoglou GD, Antoniadis AP, Koskinas KC, Chatzizisis YS. Flow and atherosclerosis in coronary bifurcations. EuroIntervention. Dec 2010;6 Suppl J:J16-23. doi:10.4244/EIJV6SUPJA4

42. Seneviratne A, Hulsmans M, Holvoet P, Monaco C. Biomechanical factors and macrophages in plaque stability. Cardiovascular Research. 2013;99(2):284-293. doi:10.1093/cvr/cvt097

43. Galis ZS, Sukhova GK, Kranzhöfer R, Clark S, Libby P. Macrophage foam cells from experimental atheroma constitutively produce matrix-degrading proteinases. Proceedings of the National Academy of Sciences. 1995;92(2):402-406. doi:10.1073/pnas.92.2.402

44. Komatsu S, Yutani C, Takahashi S, et al. Debris collected in-situ from spontaneously ruptured atherosclerotic plaque invariably contains large cholesterol crystals and evidence of activation of innate inflammation: Insights from non-obstructive general angioscopy. Atherosclerosis. Mar 10 2022;doi:10.1016/j.atherosclerosis.2022.03.010

45. Raber L, Ueki Y, Otsuka T, et al. Effect of Alirocumab Added to High-Intensity Statin Therapy on Coronary Atherosclerosis in Patients With Acute Myocardial Infarction: The PACMAN-AMI Randomized Clinical Trial. JAMA. May 10 2022;327(18):1771-1781. doi:10.1001/jama.2022.5218

46. Quillard T, Franck G, Mawson T, Folco E, Libby P. Mechanisms of erosion of atherosclerotic plaques. Current Opinion in Lipidology. 2017;28(5):434-441. doi:10.1097/mol.0000000000000440

47. Quillard T, Araújo HA, Franck G, Shvartz E, Sukhova G, Libby P. TLR2 and neutrophils potentiate endothelial stress, apoptosis and detachment: implications for superficial erosion. European Heart Journal. 2015;36(22):1394-1404. doi:10.1093/eurheartj/ehv044

48. Franck G, Mawson T, Sausen G, et al. Flow Perturbation Mediates Neutrophil Recruitment and Potentiates Endothelial Injury via TLR2 in Mice. Circulation Research. 2017;121(1):31-42. doi:10.1161/circresaha.117.310694

49. Shimonaga K, Matsushige T, Takahashi H, et al. Association of Neutrophil Extracellular Traps with plaque instability in patient with carotid artery stenosis. Ann Vasc Surg. Mar 8 2022;doi:10.1016/j.avsg.2022.02.023

50. Grover SP, Mackman N. Tissue factor in atherosclerosis and atherothrombosis. Atherosclerosis. Aug 2020;307:80-86. doi:10.1016/j.atherosclerosis.2020.06.003

51. Freynhofer MK, Bruno V, Wojta J, Huber K. The role of platelets in athero-thrombotic events. Curr Pharm Des. 2012;18(33):5197-214. doi:10.2174/138161212803251899

52. Langer HF, Daub K, Braun G, et al. Platelets Recruit Human Dendritic Cells Via Mac-1/JAM-C Interaction and Modulate Dendritic Cell Function In Vitro. Arteriosclerosis, Thrombosis, and Vascular Biology. 2007;27(6):1463-1470. doi:10.1161/atvbaha.107.141515

53. Kuijper PHM, Torres HIG, Houben LAMJ, Lammers JWJ, Zwaginga JJ, Koenderman L. P-selectin and MAC-1 mediate monocyte rolling and adhesion to ECM-bound platelets under flow conditions. Journal of Leukocyte Biology. 1998;64(4):467-473. doi:10.1002/jlb.64.4.467

54. Zago AC, Simon DI, Wang Y, et al. The importance of the interaction between leukocyte integrin Mac-1 and platelet glycoprotein Ib-a for leukocyte recruitment by platelets and for the inflammatory response to vascular injury. Arq Bras Cardiol. Jan 2008;90(1):54-63. doi:10.1590/s0066-782x2008000100009

55. Penz S, Reininger AJ, Brandl R, et al. Human atheromatous plaques stimulate thrombus formation by activating platelet glycoprotein VI. The FASEB Journal. 2005;19(8):898-909. doi:10.1096/fj.04-2748com

56. Schulz C, Penz S, Hoffmann C, et al. Platelet GPVI binds to collagenous structures in the core region of human atheromatous plaque and is critical for atheroprogression in vivo. Basic Research in Cardiology. 2008;103(4):356-367. doi:10.1007/s00395-008-0722-3

57. Martinod K, Wagner DD. Thrombosis: tangled up in NETs. Blood. 2014;123(18):2768-2776. doi:10.1182/blood-2013-10-463646

58. Franck G, Mawson TL, Folco EJ, et al. Roles of PAD4 and NETosis in Experimental Atherosclerosis and Arterial Injury. Circulation Research. 2018;123(1):33-42. doi:10.1161/circresaha.117.312494

59. Folco EJ, Mawson TL, Vromman A, et al. Neutrophil Extracellular Traps Induce Endothelial Cell Activation and Tissue Factor Production Through Interleukin-1α and Cathepsin G. Arteriosclerosis, Thrombosis, and Vascular Biology. 2018;38(8):1901-1912. doi:10.1161/atvbaha.118.311150

60. Stafford NP, Pink AE, White AE, Glenn JR, Heptinstall S. Mechanisms Involved in Adenosine Triphosphate–Induced Platelet Aggregation in Whole Blood. Arteriosclerosis, Thrombosis, and Vascular Biology. 2003;23(10):1928-1933. doi:10.1161/01.atv.0000089330.88461.d6

61. Li N, Ji Q, Hjemdahl P. Platelet-lymphocyte conjugation differs between lymphocyte subpopulations. Journal of Thrombosis and Haemostasis. 2006;4(4):874-881. doi:10.1111/j.1538-7836.2006.01817.x

62. Diacovo TG, Roth SJ, Morita CT, Rosat JP, Brenner MB, Springer TA. Interactions of human alpha/beta and gamma/delta T lymphocyte subsets in shear flow with E-selectin and P-selectin. Journal of Experimental Medicine. 1996;183(3):1193-1203. doi:10.1084/jem.183.3.1193

63. Elzey BD, Tian J, Jensen RJ, et al. Platelet-Mediated Modulation of Adaptive Immunity. Immunity. 2003;19(1):9-19. doi:10.1016/s1074-7613(03)00177-8

64. Gerdes N, Zhu L, Ersoy M, et al. Platelets regulate CD4+ T-cell differentiation via multiple chemokines in humans. Thrombosis and Haemostasis. 2011;106(08):353-362. doi:10.1160/th11-01-0020

65. Todoroki N, Watanabe Y, Akaike T, et al. Enhancement by IL-1β and IFN-γ of platelet activation: Adhesion to leukocytes via GMP-140 / padgem protein (CD62). Biochemical and Biophysical Research Communications. 1991;179(2):756-761. doi:10.1016/0006-291x(91)91881-c

66. Oleksowicz L, Paciucci PA, Zuckerman D, Colorito A, Rand JH, Holland JF. Alterations of platelet function induced by interleukin-2. J Immunother (1991). Oct 1991;10(5):363-70. doi:10.1097/00002371-199110000-00008

67. Penz S. Aktivierung von Thrombozyten durch humane atherosklerotische Plaques: Mechanismen und Inhibition. . LMU München; 2008. https://edoc.ub.uni-muenchen.de/9371/

68. Van Kruchten R, Cosemans JM, Heemskerk JW. Measurement of whole blood thrombus formation using parallel-plate flow chambers - a practical guide. Platelets. 2012;23(3):229-42. doi:10.3109/09537104.2011.630848

69. Aires RB, Soares AADSM, Gomides APM, et al. Thromboelastometry demonstrates endogenous coagulation activation in nonsevere and severe COVID-19 patients and has applicability as a decision algorithm for intervention. PLOS ONE. 2022;17(1):e0262600. doi:10.1371/journal.pone.0262600

70. Westhorpe CLV, Norman MU, Hall P, et al. Effector CD4+ T cells recognize intravascular antigen presented by patrolling monocytes. Nature Communications. 2018;9(1)doi:10.1038/s41467-018-03181-4

71. Silvain J, Collet JP, Nagaswami C, et al. Composition of coronary thrombus in acute myocardial infarction. J Am Coll Cardiol. Mar 22 2011;57(12):1359-67. doi:10.1016/j.jacc.2010.09.077

72. Niyonzima N, Halvorsen B, Sporsheim B, et al. Complement activation by cholesterol crystals triggers a subsequent cytokine response. Mol Immunol. Apr 2017;84:43-50. doi:10.1016/j.molimm.2016.09.019

73. Gravastrand CS, Steinkjer B, Halvorsen B, et al. Cholesterol Crystals Induce Coagulation Activation through Complement-Dependent Expression of Monocytic Tissue Factor. The Journal of Immunology. 2019;203(4):853-863. doi:10.4049/jimmunol.1900503

74. Whiting D, Dinardo JA. TEG and ROTEM: Technology and clinical applications. American Journal of Hematology. 2014;89(2):228-232. doi:10.1002/ajh.23599

75. Tatsumi K, Mackman N. Tissue Factor and Atherothrombosis. Journal of Atherosclerosis and Thrombosis. 2015;22(6):543-549. doi:10.5551/jat.30940

76. Kuijpers MJE, Van Der Meijden PEJ, Feijge MAH, et al. Factor XII Regulates the Pathological Process of Thrombus Formation on Ruptured Plaques. Arteriosclerosis, Thrombosis, and Vascular Biology. 2014;34(8):1674-1680. doi:10.1161/atvbaha.114.303315

77. Hansson GRK, Jonasson L. The Discovery of Cellular Immunity in the Atherosclerotic Plaque. Arteriosclerosis, Thrombosis, and Vascular Biology. 2009;29(11):1714-1717. doi:10.1161/atvbaha.108.179713

78. Dargazanli C, Rigau V, Eker O, et al. High CD3+ Cells in Intracranial Thrombi Represent a Biomarker of Atherothrombotic Stroke. PLOS ONE. 2016;11(5):e0154945. doi:10.1371/journal.pone.0154945

79. Marchini T, Hansen S, Wolf D. ApoB-Specific CD4+ T Cells in Mouse and Human Atherosclerosis. Cells. 2021;10(2):446. doi:10.3390/cells10020446

80. Reininger AJ, Bernlochner I, Penz SM, et al. A 2-Step Mechanism of Arterial Thrombus Formation Induced by Human Atherosclerotic Plaques. Journal of the American College of Cardiology. 2010;55(11):1147-1158. doi:10.1016/j.jacc.2009.11.051

81. Reininger AJ. Thrombusformation im Blutfluss. In: Pötzsch B, Madlener K, eds. Hämostaseologie. Springer Berlin Heidelberg; 2010:73-80.

82. Alshehri FSM, Whyte CS, Tuncay A, Williams M-L, Wilson HM, Mutch NJ. Monocytes Expose Factor XIII-A and Stabilize Thrombi against Fibrinolytic Degradation. International Journal of Molecular Sciences. 2021;22(12):6591. doi:10.3390/ijms22126591

83. Kratofil RM, Kubes P, Deniset JF. Monocyte Conversion During Inflammation and Injury. Arteriosclerosis, Thrombosis, and Vascular Biology. 2017;37(1):35-42. doi:10.1161/atvbaha.116.308198

84. Morrow GB, Whyte CS, Mutch NJ. A Serpin With a Finger in Many PAIs: PAI-1's Central Function in Thromboinflammation and Cardiovascular Disease. Front Cardiovasc Med. 2021;8:653655. doi:10.3389/fcvm.2021.653655

85. Tjärnlund-Wolf A, Brogren H, Lo EH, Wang X. Plasminogen Activator Inhibitor-1 and Thrombotic Cerebrovascular Diseases. Stroke. 2012;43(10):2833-2839. doi:10.1161/strokeaha.111.622217

86. Fay WP, Garg N, Sunkar M. Vascular Functions of the Plasminogen Activation System. Arteriosclerosis, Thrombosis, and Vascular Biology. 2007;27(6):1231-1237. doi:10.1161/atvbaha.107.140046

87. Juhan-Vague I, Pyke SD, Alessi MC, Jespersen J, Haverkate F, Thompson SG. Fibrinolytic factors and the risk of myocardial infarction or sudden death in patients with angina pectoris. ECAT Study Group. European Concerted Action on Thrombosis and Disabilities. Circulation. Nov 1 1996;94(9):2057-63. doi:10.1161/01.cir.94.9.2057

88. Nagai N, Suzuki Y, Van Hoef B, Lijnen HR, Collen D. Effects of plasminogen activator inhibitor-1 on ischemic brain injury in permanent and thrombotic middle cerebral artery occlusion models in mice. Journal of Thrombosis and Haemostasis. 2005;3(7):1379-1384. doi:10.1111/j.1538-7836.2005.01466.x

89. Luttun A, Lupu F, Storkebaum E, et al. Lack of Plasminogen Activator Inhibitor-1 Promotes Growth and Abnormal Matrix Remodeling of Advanced Atherosclerotic Plaques in Apolipoprotein E–Deficient Mice. Arteriosclerosis, Thrombosis, and Vascular Biology. 2002;22(3):499-505. doi:10.1161/hq0302.104529

## VII. Acknowledgements

Firstly, I would like to express my deepest gratitude to Prof. Dr. med Bernd Engelmann for giving me the opportunity to work in his research group on this interesting topic. I am incredibly grateful for his guidance and insightful discussions at every step of the project and for his constructive criticism, which pushed me to improve the ways I think about and carry out scientific work. I thank him for opening the world of research to me and laying the groundwork for a future scientific career.

Next, I would like to thank Prof. Dr. med. Daniel Teupser, the director of the Institut für Laboratoriumsmedizin, Klinikum der Universität München, Ludwig-Maximilians-Universität (LMU) for supporting my doctoral thesis.

I want to express my thanks to all the people who worked in the lab with me and introduced me to the world of science. Thank you for teaching me new techniques and ways to think and improvise. Thank you for always being there, day or night, ready to assist whenever help was needed, and thank you for helping me reflect on my ideas, contemplate experiments, and interpret new findings. Special thanks to Mona Wohlrab, Manovriti Thakur, Junfu Luo, Torben Lang Heinrich, and Michael Völkl.

I also want to express my gratitude to Prof. Dr. med. Steffen Massberg (Medizinische Klinik und Poliklinik I, Klinikum der Universität München) and his research group at the Walter Brendel research centre for the beneficial cooperation.

I would also like to thank Prof. Dr. med. Christian Schulz and Mrs. Ana Titova, for their assistance and insightful discussions, as well as their expertise regarding FACS and cell stainings. Greatest of thanks to Dr. Hellen Ishikawa-Ankerhold and Dominic Adam van den Heuvel for all the guidance whenever I encountered problems and for our cooperation regarding flow-chamber and animal experiments.

And lastly, I would like to thank all my friends and family who supported and motivated me throughout this journey, encouraging me always to give my best and to persevere, no matter the obstacles.

## VIII. Affidavit

LMU LUDWIG-MAXIMILIANS-UNIVERSITÄT MÜNCHEN | Promotionsbüro Medizinische Fakultät | MMRS

**Eidesstattliche Versicherung**

Radev, Marian

Name, Vorname

Ich erkläre hiermit an Eides statt, dass ich die vorliegende Dissertation mit dem Titel:

**Involvement of immune cells in coagulation activated by atherosclerotic plaques**

selbständig verfasst, mich außer der angegebenen keiner weiteren Hilfsmittel bedient und alle Erkenntnisse, die aus dem Schrifttum ganz oder annähernd übernommen sind, als solche kenntlich gemacht und nach ihrer Herkunft unter Bezeichnung der Fundstelle einzeln nachgewiesen habe.

Ich erkläre des Weiteren, dass die hier vorgelegte Dissertation nicht in gleicher oder in ähnlicher Form bei einer anderen Stelle zur Erlangung eines akademischen Grades eingereicht wurde.

München, 16.05.2025 Marian Radev

Ort, Datum Unterschrift Doktorandin bzw. Doktorand

# Publications

Radeva E, Marinova-Takorova M, Radev M. A survey among dental students on their knowledge on antibiotic therapy of endodontic infection. 2019 [SYLWAN., 163(3)]